Cold Regions Research and Engineering Laboratory

US Army Corps of Engineers
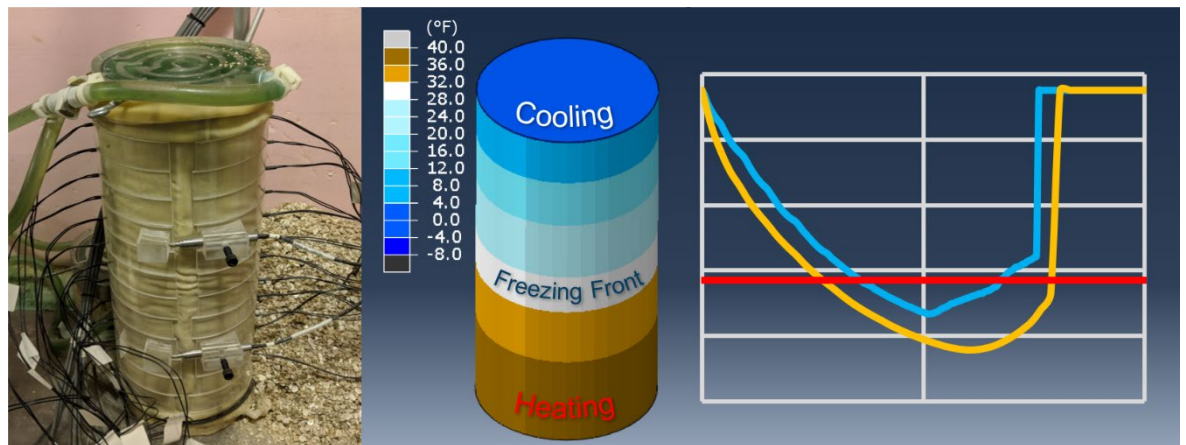Engineer Research and Development Center

ERDC
ENGINEER RESEARCH & DEVELOPMENT CENTER

Innovative Construction Materials for the Arctic

Frost-Depth Penetration and Frost Heave in Frost-Susceptible Soils

Wade A. Lein, Scott Michael L. Slone, Charles E. Smith Jr., Andrew P. Bernier, and Jared I. Oren

November 2019

The U.S. Army Engineer Research and Development Center (ERDC) solves the nation's toughest engineering and environmental challenges. ERDC develops innovative solutions in civil and military engineering, geospatial sciences, water resources, and environmental sciences for the Army, the Department of Defense, civilian agencies, and our nation's public good. Find out more at www.erdc.usace.army.mil.

To search for other technical reports published by ERDC, visit the ERDC online library at http://acwc.sdp.sirsi.net/client/default.

Frost-Depth Penetration and Frost Heave in Frost-Susceptible Soils

Wade A. Lein, Scott Michael L. Slone, Charles E. Smith Jr., Andrew P. Bernier, and Jared I. Oren

U.S. Army Engineer Research and Development Center (ERDC)
Cold Regions Research and Engineering Laboratory (CRREL)
72 Lyme Road
Hanover, NH 03755-1290

Final Report

Abstract

The natural freezing and thawing of soils dramatically affects their thermal and mechanical properties. This can have destructive effects on structures built on those soils.

This study developed a thermodynamic finite element model using multiple frost-susceptible soil types. It measured thermal conductivity and temperature through several freeze–thaw cycles. We identified moisture migration as likely the most significant factor in frost heave and frost penetration. Additionally, the thermal conductivity increased near the freezing front across all samples. For example, the thermal conductivity for ML (low-plasticity silt) soils rose from 301 to 357 milliBtu/(hr*ft*°F), which appeared to correspond to where the moisture concentrated and ice formation was highest.

Our experimental results guided model development, where thermal parameters changed with respect to temperature, ice, and moisture during freeze–thaw cycles. Using dynamic thermal parameters improved frost-depth prediction compared to the standard Modified Berggren equation. For our tested conditions, the equation had an error of 2.2 in. for a frost depth of 8 in. while our model had an error of 1.4 in.

These developments are important to airfield runway and general pavements design and maintenance in frost-affected regions. The findings will allow more accurate predictions of frost depth and deflection.

Contents

Figures and Tables

Figures

Tables

Preface

Acronyms and Abbreviations

CBR	California Bearing Ratio
CH	High-Plasticity Clay
CL	Low-Plasticity Clay
CRREL	U.S. Army Cold Regions Research and Engineering Laboratory
EICM	Enhanced Integrated Climatic Model
ERDC	Engineer Research and Development Center
FAIR	Frost-Area Index of Rigidity
FASSI	Frost-Area Soil Strength Index
FEA	Finite Element Analysis
FEM	Finite Element Model
LDVT	Linear Variable Differential Transformer
MBLS	ModBerg Layered Solution
MEPD	Mechanistic-Empirical Pavement Design
ML	Low-Plasticity Silt
ModBerg	Modified Berggren
NA	Not Available
NR	Noncohesive
NP	Inconclusive
OMC	Optimum Moisture Content
PCASE	Pavement-Transportation Computer Assisted Structural Engineering
SC	Clayey Sands
SFDD	Surface Freezing Degree-Days
SM	Sands with Fines
SP	Poorly Graded Silty Sands

Unit Conversion Factors

Multiply	By	To Obtain
British thermal units (International Table)	1,055.056	joules
degrees Fahrenheit	(F-32)/1.8	degrees Celsius
feet	0.3048	meters
inches	0.0254	meters
pounds (mass)	0.45359237	kilograms

1 Introduction

As soils freeze and thaw, they go from natural moisture conditions to frozen conditions. Eventually when the soil thaws, it will return to natural moisture conditions. This return is a critical phase change as the depth of the frozen layers will affect the soil's residual strength and the possible deformation in the soil layers. This deformation can devastate structures such as roadways, foundations, and embankments. U.S. Army Cold Regions Research and Engineering Laboratory (CRREL) has extensively researched this topic. Some of the research suggests that a finite element model (FEM) would be the next step in predicting frost-depth penetration.

In this testing procedure, our team set out to capture the depth of frost penetration and to measure the soil thermal properties in situ during multiple freeze and thaw cycles to guide future model development. The soil materials selected for testing varied from medium to highly frost susceptible to account for the bulk of materials affected by frost-depth penetration.

Guided by the results obtained from cyclic freezing and thawing of the above frost susceptible soils, we developed a thermodynamic FEM capable of changing its local soil thermal properties as it goes through freezing and thaw just as in experiment. This paper examines the early data and explores the observed trends of the data. This paper also incorporates the first phase of a finite element frost-depth-penetration model.

1.1 Background

1.1.1 Current frost-depth models

Numerous variables affect the penetration of frost into susceptible soils. Just as many methods exist to define the depth of said penetration. The Mechanistic-Empirical Pavement Design (MEPD) method, a standard with many departments of transportation, uses an Enhanced Integrated Climatic Model (EICM) to predict the deformation on pavements, while the military uses the Pavement-Transportation Computer Assisted Structural Engineering (PCASE) program. The ECIM, when combined with a soil water characteristic curve, can be used to predict California Bearing Ratios (CBRs) and other mechanical properties for pavement layers. Therefore,

accurately predicting soil water content is important for soil strength prediction, although our research does not expressly explore the MEPD method or seek to replicate it, due to the existing dependence by the military on the PCASE program.

PCASE uses the Modified Berggren (ModBerg) equation, which is a modification of the Stefan equation (Aldrich and Paynter 1953). The ModBerg equation, in theory, is a very large and complex equation, requiring nine input variables, such as the thermal conductivities for frozen and unfrozen soils. In practice, many of these variables are thermal properties and can be determined by inherent soil properties or are weather properties such as the frost and thaw indexes, which do not drastically change for any specific location (Zarlinget al. 1991).

To address this, PCASE requires the user to instead provide more easily determined properties to infer the thermal properties. The user provides the soil's dry unit weight, soil type, and moisture content; and these values are used to calculate the thermal properties based on empirical relationships. For the weather properties, the user provides the relevant state or nation and then selects from a list of provided weather stations one near where their pavement is going to be built. PCASE then opens an included database to retrieve data on the mean annual temperature, length of frost and thaw seasons, index, etc. This information then passes to a self-contained program inside PCASE that calculates the remaining inputs for the ModBerg equation; and, dependent on which is a more significant effect, the equation outputs the frost or thaw depth. The self-contained program then provides the resulting penetration of frost or thaw to the rest of PCASE so it can define the required thickness for the pavement design to be frost resistant (Bianchini and Gonzalez 2012).

1.1.2 Origin of the PCASE frost penetration model

The ModBerg equation is visually similar to the Stefan equation, with the only change being it is multiplied by an additional correction factor, which provides much of the equation's accuracy (Aldrich and Paynter 1953) (Zarling et al. 1991) (Soil Engineering Division 1957) (Departments of the Army and the Air Force 1988). The Stefan equation is notoriously inaccurate, in part because it does not account for the soil's volumetric heat capacity, representing frost depth as a simple diffusion-like relationship with freezing temperature and time (Zarling et al. 1991). The ModBerg equation addresses this by incorporating soil thermal parameters. However, these

are incorporated into a transcendental equation that cannot be solved analytically and has different forms depending on if it is finding the solution for the soil freezing state or the soil thawing state. Equation (1) shows the ModBerg equation and the solution for the correction factor, γ, in the freezing state:

$$X = \gamma \sqrt{\frac{96kI}{v_s c_f}},$$

where γ is solved by

$$\frac{e^{-\frac{\gamma^2}{4\kappa_f}}}{\mathrm{erf}\left(\frac{\gamma}{2\sqrt{\kappa_f}}\right)} - \frac{T_g}{T_s}\frac{k_u}{k_f}\sqrt{\frac{\kappa_f}{\kappa_u}}\frac{e^{-\frac{\kappa_f}{\kappa_u}\left(\frac{\gamma}{2\sqrt{\kappa_f}}\right)^2}}{erfc\left(\sqrt{\frac{\kappa_f}{\kappa_u}}\frac{\gamma}{2\sqrt{\kappa_f}}\right)} = \frac{\gamma}{2\sqrt{\kappa_f}}\frac{\sqrt{\pi}}{\left(\frac{c_f T_s}{L}\right)}, \tag{1}$$

where

$$
\begin{aligned}
X &= \text{the frost depth;} \\
k &= \text{the thermal conductivity of the soil in its current state;} \\
I &= \text{the freezing/thaw index;} \\
v_s &= \text{the absolute difference between the mean ground temperature} \\
&\quad\text{and the water's freezing point;} \\
c &= \text{the volumetric heat capacity;} \\
\gamma &= \text{the correction factor;} \\
\kappa &= \text{the thermal diffusivity;} \\
L &= \text{the volumetric latent heat;} \\
T_g &= \text{the initial ground temperature;} \\
T_s &= \text{the constant surface temperature; and} \\
u \text{ and } f &= \text{the parameters for unfrozen and frozen soils, respectively.}
\end{aligned}
$$

The thawing-state version is identical except the u and f parameters are reversed (i.e., the term k_u/k_f in the freezing state version becomes k_f/k_u in the thawing-state version).

There is the possibility of solving equation (1) numerically, but PCASE instead uses an approximation that has a deviation of at most 5% from the numerical error. This approximation assumes that there is not a dramatic difference between the thermal properties of frozen and unfrozen soils. In reality, there can be significant differences that lead to large errors when

ratios vary amount from 1, such as the ratio of thermal diffusivities, which can vary from 0.8 to 1.7 for typical soils. This incorrect assumption about thermal properties of soils tends to overestimate thermal variance, which increases the correction factor, and underestimate the fusion parameter, which decreases the correction factor, the intention being that these two errors would cancel each other out (Zarling et al. 1991). There is not sufficient evidence to confirm this claim; and in practice, ModBerg tends to overestimate frost depth (Rajaei and Baladi 2015). Furthermore, the equation requires the average thermal conductivity of frozen and unfrozen soils, which will predict a depth of frost smaller than that using just the frozen soil thermal conductivity. This trend is reversed for the opposite case in predicting the depth of thaw (Zarling et al. 1991).

Alongside the ModBerg equation is the ModBerg Layered Solution (MBLS). It is intended for layered systems with varying thermal properties and is more applicable to pavement design. The MBLS calculates the number of surface freezing degree-days (SFDD) to completely freeze a layer of predetermined thickness. This is subtracted from the total SFDD available until the SFDD required to freeze a layer is more than the available SFDD. The depth of this final layer is adjusted until the difference between required and available SFDD is less than 10°F-Days. This final layer depth plus the thicknesses of the above layers is the total frost penetration for the pavement design, allowing it to be adjusted as needed. While it effectively accounts for the potentially varied thermal properties of different pavement layer types, an inherent flaw in the MBLS is that it does not account for the properties of the layer below the final layer or any layer aside from the one currently being calculated. With the MBLS, the same frost-depth penetration would be calculated for three systems with different layers, such as the bed of gravel, a layer of fine silt, or a thick insulation layer, provided the frost does not penetrate into these layers (Bianchini and Gonzalez 2012).

Zarling et al. (1991) recommended that finite element analysis (FEA) would be the most appropriate method to verify ModBerg's predictions, especially in cases where knowing the depth accurately is critically important. To verify this claim, Zarling et al. (1991) compared the version of ModBerg that would eventually be used in PCASE to several other methods, including computational methods. The two computational methods were 2D Heat Conduction, an FEM program that represented frozen and

unfrozen soil as separate elements, and Berg2, empirically driven and calibrated for Alaskan weather and soil behavior (Braley and Connor 1989). When compared to multiple pavement designs in Alaska, ModBerg overpredicted frost and underpredicted thaw depths when compared to the computational models. 2D Heat Conduction was not as accurate as Berg2 but was more accurate than ModBerg. It achieved this improvement using a computational load that would be trivial on today's computers (Zarling et al. 1991).

1.1.3 Subgrade mechanical strength factors

There are two general methods for determining pavement thickness in cold regions: the limited subgrade penetration method and the reduced subgrade strength method. The limited subgrade penetration method involves reducing the amount of pavement distortion due to frost heave to a minimal level by increasing the pavement base thickness to a sufficient level. Increasing pavement thickness minimizes frost penetration into the subgrade (Berg and Johnson 1983). However, this method is uneconomical in practice, requiring more material than necessary when compared to other methods. The other option, the reduced subgrade strength method, assumes a lower-than-average design strength for the pavement, accounting for periods of the year when the subgrade is substantially weakened, such as during thawing seasons. This route is more economical but requires replacement of material properties with values specific to the situation. The method assumes horizontal uniformity in the subgrade structure, which must be maintained to guarantee that this method works (Guyer 2013).

The reduced subgrade strength method replaces the strengths of flexible and rigid pavements with new values, known as the Frost-Area Soil Strength Index (FASSI) and the Frost-Area Index of Rigidity (FAIR). The FASSI/FAIR factors are the average strengths of these pavements over the course of several seasons, approximately representing their strength in any season. FASSI serves as a replacement for the CBR value of flexible pavements even though it is not a CBR value itself. It is solely dependent on the subgrade soil's frost susceptibility, with highly susceptible soils having a FASSI value of 9.0 even if their CBR is different. Likewise, FAIR replaces CBR's mechanical analogue in rigid pavements, although it is an equation based on pavement thickness and dependent on construction conditions. In flexible pavements, it is a simple process of replacing the subgrade strengths with their appropriate FASSI values. The pavement thickness

and frost penetration depth are calculated as normal, and the new thicknesses based on the reduced subgrade strength method are used, unless the original thicknesses are larger. For rigid pavements, the FAIR factor is calculated from base layer thickness (U.S. Army Corps of Engineers 1984). To use this method, the base thickness must be equal to the rigid slab but not thinner than 4 in., with greater thicknesses affecting pavement rigidity in the positive. The strength of the slab is determined from a graphical relationship between base thickness and FAIR factor, dependent on the soil type. As the base thickness increases, the strength of the pavement structure increases. The thickness is increased to an optimum level where the strength is sufficient for the expected pavement life, cost, and other factors. However, neither the FASSI nor FAIR factors take into account moisture content or soil density, as their values are defined entirely on the soil classification (Guyer 2013; Berg and Johnson 1983).

1.1.4 Finite element modelling of pavements

Early pavement modelling studies recommended using finite element analysis to better predict material properties, internal stresses, and thermal parameters (Zarling et al. 1991). This was wise advice as FEM accuracy has improved over time (Holanda et al. 2006; Yassenn et al. 2015). As computational resources increase in availability, the precision of models can improve dramatically. A potential improvement for these models, some of which are one-dimensional linear representations of pavement layers, is to have multidimensionality. Properties such as shear stress and interlayer bonding can only be accurately represented in two- or three-dimensional model (Holanda et al. 2006; Hammons 1998). There are several options for potential multidimensional pavement models, the most efficient option being tuning an existing finite element analysis model to pavement and soil materials properties. One potential choice is ABAQUS (Kim 2007; Leonardi 2014), which we will discuss in later sections. FEMs have successfully modeled not just the results of mechanical deformation and wear, such as from traffic, but also pavement degradation from thermal effects (Ban et al. 2017).

1.1.5 Soil types

Four main soil types are defined as frost susceptible. The coarsest gradation that has a slight-to-high frost action potential is silty sands that are poorly graded (e.g., SP) and clayey sands (e.g., SC). Soils with gradations larger than this are unable to retain moisture in the pore space of the soil.

The next gradations that have medium-to-very-high frost action potential are silts and clays with a liquid limit less than 50. This encompasses materials from silty gravels to clayey sands. These materials have smaller pores and thus are able to have more pore water as the freezing water makes the pore space expand in volume; and when the water thaws, the material is less dense. The freezing and thawing conditions are the most vulnerable times for these soils. The last category for soils is those with medium-to-very-high frost action potential, which are silty clays with a liquid limit greater than 50. These are highly plastic materials, such as fat clays. These materials have the highest ability to expand and compress. They also have very-poor-to-impervious drainage characteristics. Once moisture is in the material, it does not come out easily and can exhibit poor strength when subjected to frost actions (American Association of State Highway and Transportation Officials 2008, 86).

1.1.6 Input variables

Previous researchers have used several properties to characterize and model soils, such as dry density, water content, temperature gradient, and specific gravity (Shastri and Sanchez 2014, 3480). To model moisture flow, their models incorporated parameters for pressure and soil permeability (Shastri and Sanchez 2014, 3482). Shoop et al. (2005, 3) used a Capped Drucker-Prager plasticity model within the FEM program ABAQUS. Plastic models are for modeling materials that deform plastically, and this model could be expanded to include the elastic state of the soil. In the thawing state, the elastic zone of the soils is very minimal. The model parameters include material cohesion, the material angle of friction, cap eccentricity, slopes of the loading (compression) and unloading (elastic) lines, Young's modulus, and Poisson's ratio (Shoop et al. 2005, 3). Shoop's team also measured gradation, moisture content, CBR, triaxial shear, and void ratio, although their parameters did not directly guide the model.

The RIGIDICE model developed by CRREL uses thermal conductivity, hydraulic conductivity, heave rate, the penetration rate of the freezing point, porosity, and change in capillary pressure (Black 1995). This model accounts for the effects of ice lenses, which could cause secondary frost heave. This secondary frost heave is related to freezing and thawing in that, as a void space freezes then thaws over and over, the area expands and develops ice inclusions. This model was intended for use below pavements (Black 1995, 2).

Guymon et al. (1993) defined soils by frost group, dry density, void ratio, and saturated permeability and used them as inputs to find Gardner's coefficients for the different soil types. The Gardner's coefficients are multipliers of pore pressure as it relates to the soil's moisture conditions. These coefficients were available for unsaturated soils and depend on the soil's moisture content. Guymon et al. (1993) also used specific heat and thermal conductivity parameters.

Bigl and Shoop (1994, 2) coupled the heat and moisture flow in a new model where they used the Gardner coefficients of moisture along with the hydraulic conductivity, porosity, density, thermal conductivity, volumetric heat capacity, and E factor. The E factor is an empirically derived constant based on saturated hydraulic conductivity. The material used to validate their model was sands with fines (SM) (Bigl and Shoop 1994). They recommended that the soil does not have to be completely saturated for frost heave to occur.

Berg et al. (1980) developed a one-dimensional finite difference model. The key external factors that affected the model were loading and surcharge. Following these factors, the climate had a great effect on the frost depth. They used latitude, altitude, air temperature, precipitation, sunshine, wind, humidity, and evaporation to define the climatic external forces on the system. The last external consideration was the land cover; and the values they used were vegetation, snow, and pavement. They also developed an FEM to predict frost heave. Thanks to their work, many of the parameters originally calculated using empirical equations can now be directly measured. They did state that the most critical factors in their model were porosity and hydraulic conductivity of the soil (Berg et al. 1980, 19). These properties change as the soil freezes and thaws.

1.1.7 Literature discussion

The above research made clear that our primary focus should be on improving a FEM solution for frost-depth penetration, and that experimentation should focus on determining the correct thermal properties of soils.

The first focus of research was on external properties effecting freezing and on improving the accuracy of that information. We specifically focused on the databases of PCASE as it will serve as a major framework for our future efforts. PCASE has the user select the location of the building site. In making this selection, the user is selecting several properties from an

available database, such as the elevation, humidity, air temperature, precipitation, sunshine, wind speed, and evaporation. We either measured or controlled these properties during testing.

The internal elements that affect the soil's ability to freeze are gradation, porosity, thermal conductivity, moisture content, hydraulic conductivity, specific gravity, void ratio, particle shape, internal temperature, and volume change. The PCASE program uses frost depth to define soil-strength reducing factors, like the FASSI/FAIR factors described above.

1.2 Objectives

To improve the prediction of frost-depth penetration and estimates of in situ thermal and mechanical properties of soils, it was clear that a FEM-guided method was the most effective route, based on reported successes from literature. We focused on improving the frost-depth prediction of the PCASE design software, which uses the ModBerg equation. While achievable, designing an FEM with higher accuracy than the ModBerg equation would require experimental verification of its guiding parameters.

1.3 Approach

To achieve our above objective, we focused on obtaining the necessary material properties of various frost-susceptible soils and identifying if those properties change as the soil freezes and thaws. This report first describes the soil selection and how samples were prepared. We discuss the individual material properties and what testing standards we used to determine them. We later go into the specific details of our results, focusing on the freeze–thaw tests for the bulk of the report, where we determine both frost-depth penetration and thermal conductivity. Finally we discuss our computational model, which incorporates these and other parameters. Comparisons between this model and the ModBerg equation verify if it is a capable alternative to the equation.

2   Test Design

2.1   Research test

To verify the current ModBerg equation and to train a novel FEM for comparison, we targeted four frost-susceptible soil types used in construction. The selected soils were a poorly graded silty sand (SP), low-plasticity silt (ML), low-plasticity clay (CL), and a high-plasticity clay (CH), using the Unified Soil Classification System's definitions for soil types. These four soil types are classified as low to very high in terms of frost susceptibility, with silts and clays having higher frost susceptibility. CL soils are clays with a liquid limit lower than 50, and CH soils are clays with a liquid limit above 50. Characterization of soils included liquid limit, moisture-density curves, and gradations.

Once we knew the materials properties, we compacted the samples at 95% of a modified proctor maximum density with a moisture content within 2% of optimum. This mimicked compaction of soils in highway construction. To simulate lower compaction effort, we prepared a second set of samples with nine-tenths of the moisture content of the first. Additionally, for the frost-heave tests, we made a third set with the moisture content of the first set but with a source of free water positioned underneath the sample. Moisture would travel up through the sample by capillary action, simulating a natural water source under the soil. Moisture contents were determined according to ASTM D2216 (2019). Each sample had its moisture determined before and after the tests as required by the individual ASTMs for those tests.

The characterizations of all materials included soil gradations with a hydrometer as gradations play a large part in the permeability and potential frost action of a soil. PCASE uses CBR tests for the design and evaluation of pavements. Therefore, we performed standard CBR testing on all soils, which will provide data sets for future PCASE calibration and correlation.

To accurately predict thermal properties, We measured thermal conductivity continuously as the soils froze, as soil thermal conductivity is dependent on the ratio of frozen to unfrozen water. Thermal conductivity is currently part of the ModBerg equation as described previously; but in PCASE, it is a calculated parameter that is based on an empirical relation-

ship between only soil density and moisture content. To rule out any potential errors this empirical method may cause, the PCASE method was not used to calculate our thermal conductivity values, which were obtained directly through thermistor sensors. The results were collected for use in our FEM so that the model soil's thermal properties would change as it froze, mimicking experimental results.

The frost-heave test allowed a direct measurement on laboratory samples of the potential amount of frost heave and depth of frost penetration. Embedded in the frost-heave sample were temperature and thermal conductivity sensors. To simplify model development, tests were conducted with no surcharge weight, which normally represents a layer of pavement over the soil. Samples were 12 in. high with a 6 in. diameter and were frozen by placing a cold plate on top of the samples and freezing from the top down to replicate field conditions. Radial linear variable differential transformers were placed on the side of the samples at distances of 4 and 10 in. from the cold plate to understand soil displacement as it freezes.

2.2   Test plan

This study included multiple separate tests of the soils' thermal and mechanical properties. This section describes the different parameters measured, the ASTM standards used to guide those experiments, shown in Table 1, and the reason for their measurement.

Table 1. Testing setup for the modified frost-heave test.

Parameter	ASTM Standards
Moisture	D2216, D6026
Liquid Limit / Plastic Limit	D4318
California Bearing Ratio	D1883
Thermal Conductivity	D5334, D6026
Gradation with Hydrometer	D7928
Porosity	D7063
Frost Heave	D5918, D2940, D1883, D2216
Frost Depth	D5918

The method for moisture involved determining the appropriate moisture content within an accuracy of 1%. We recorded the mass of the clean and dry specimen container and lid and collected a suitable sample that was homogenous and representative of the water condition of the entire system. The samples were retrieved from a soil stockpile that was guaranteed to be

homogeneous before acquisition and measurement. We recorded the mass of container and sample and placed it in a drying oven at 110 ± 5°C for at least 2 hours. We checked the weight, then repeated the heating process if the difference in mass was greater than the method accuracy limit of 1%. If the mass was less than method limit, then the specimen was considered to be finished drying. We determined the water content using a standard equation based on the masses of the container and moist/dry specimens.

Measurement of liquid limit used the wet preparation and multipoint sampling options from ASTM D4318 (2017a). Samples were prepared based on their particle size and ability to pass through a standard sieve. We placed prepared samples in a liquid limit dish with a standard gap constructed in the sample. The dish was dropped multiple times until the gap closed. We increased the water content multiple times to identify the water contents best associated with 15–25, 20–30, and 25–35 drops, with water content determined using the same method as above for soil moisture. A linear fit was made through the three points on a logarithmic graph. Liquid limit was defined by the point on the linear fit matching 25 drops.

Samples for measuring CBR were prepared at a range of water contents relevant to the study to identify the optimum moisture content (OMC). A penetration piston was mounted on the sample with a predetermined loading weight defined by the standard, with a strain rate of 0.05 in./min. We used the recorded loads to calculate the load-penetration curve, bearing ratio, and other factors required to determine the CBR.

Soil gradation was determined by mixing soil samples and then separating out portions into a free-floating particle solution, which was placed in a soil hydrometer. Hydrometer parameters were recorded over the course of 24 hours, with the end result being a distribution of particle mass percentage versus particle diameter.

To measure porosity, we placed compacted samples matching ASTM specifications inside a plastic bag, which was evacuated of all air and vacuum sealed. Sample density was recorded via water displacement. The bag was punctured while in water, and the resulting displacement of water was recorded. The porosity was determined based on the difference in the initial and final volume displacements.

To determine frost depth and frost heave, samples were prepared by compacting soil into a standard shape, a 14.4 in. tall cylinder with a 6 in. diameter. The sample was placed between two heat sources, with temperatures of heat sources adjusted every 24 hour, deviating from the ASTM standard to simplify the data input for the model as the ASTM standard's values were intended to fully freeze a smaller sample. This resulted in one freeze–thaw cycle every 48 hours, ending with the sample thawing. Each sample underwent multiple freeze–thaw cycles, depending on external limitations of power supply and cold room access. To record frost depth, we placed 12 thermal probes in the sample initially 0.6 in from the surface and then every 1.2 in. down the sample for a total of 12 probes. Frost depth was back-calculated from soil temperature, with frost-depth position interpolated between the two probes closest to freezing temperature. A linear variable differential transformer (LVDT) positioned over each sample measured frost heave of each sample, with radial heave measured by a pair of similar probes alongside the sample diameter. Figure 1 shows the testing setup. The letter A represents the thermal probes. B represents the thermal conductivity thermistors. C illustrates the cooling and heating glycol plate and was the location of the vertical LVDT for measuring frost heave. D shows the location of the radial LVDTs. E represents the bottom plate that was held at a constant 40°F.

Figure 1. Testing setup for the modified frost-heave test.
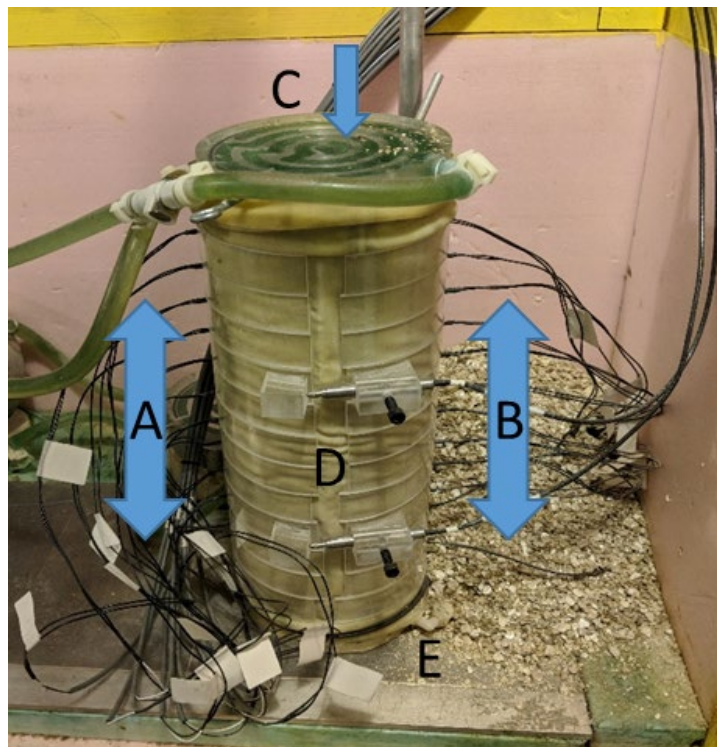
The frost-heave test was conducted in three moisture conditions: one at OMC and maximum density, a second at a moisture content 10% lower than OMC (OMC – 10%, i.e., for an OMC of 20%, this would be 18%), and a third at OMC + free water available at the bottom of the sample. No pressure head or additional weight was applied, as that might induce additional moisture migration. With both of these additional effects eliminated, all moisture migration in the frost-heave test would be from capillary and frost action. OMC was defined as where density dropped off significantly on a moisture content curve.

We recorded thermal conductivity using a modification of the standard measurement method (Atkins and Wright 1990). A thin probe used to approximate an infinite heating source was inserted to the sample. A known current was applied to the probe, and the resulting change in temperature was measured at the end of 5 minutes, then after another 5 minutes to record the return to equilibrium. Initial calibration with the various soil types found that 5 minutes was sufficient both to suitably heat and then to reequilibrate the sample. The difference in temperature was used to calculate thermal temperature. Overall, 12 probes were placed in soil samples before frost-heave and frost-depth measurements, with their locations matching thermal probe depths but on the opposite side of the cylindrical samples.

Table 2 shows the test matrix for the PCASE frost effects verifications.

Table 2. PCASE frost effects test matrix and number of tests performed.

Sample Type		SP	ML	Clay (LL<50) (CL)	Clay (LL>50) (CH)
Moisture-Density Curve		1	1	1	1
Gradation w/Hydrometer		1	1	1	1
Atterberg Limits		1	1	1	1
Porosity	Frozen	3	3	3	3
	Thawed	3	3	3	3
CBR	Frozen	2	2	2	2
	Thawed	6	6	6	6
Frost Heave	OMC	2	2	2	2
	OMC – 10%	2	2	2	2
	OCM + Free Water	2	2	2	2

3 Results and Discussion

Figures 2 through 5 illustrate the time versus temperature for all four soil types completed. The thermal and conductivity probes were labeled T1 through T12. T1 starts at the top of the sample, and T12 was located at the bottom of the sample, per the earlier definition of probe locations. Figures 6 through 9 are the thermal conductivity of the soil types as they went through the frost cycles. It is of note that some frost tests were carried out longer as power supply and cold room access permitted to determine if the thermal conductivity would continue to increase with the number of freezing cycles. This resulted in some tests having only two complete freeze–thaw cycles, while others had up to six.

3.1 Soil temperature, frost depth, and frost heave

As shown in the Figures 2 through 5, the T1 thermal probe was the coldest, which was logical as it was closest to the top of the sample and thus the primary cooling source. The T12 thermistor on the bottom had the smallest temperature change, which was also logical as it was the farthest away from the cooling source in all cases. The middle layers thawed the slowest and dwelled near freezing the longest, which could be due to the moisture migration. As soil freezes, moisture migrates towards the freezing front, which can be fast in soils like silt or slow in soils like clays. Once the sample starts to thaw the moisture continues to migrate towards the frozen layer from the top and the bottom of the sample. During this thaw state, the soil becomes saturated with moisture that flows towards the frozen layer. Figure 14 illustrates this mechanism. The samples with free water available did not get as cold due to the impact of additional moisture on thermal properties. In addition, the samples tended to obtain lower temperatures during subsequent cycles after the first, suggesting that the moisture flow is causing permanent changes in thermal properties.

In Figure 3, the low-plasticity clay exhibited freezing properties similar to the low-plasticity silt. Low-plasticity clay had a similar pattern of increasingly lower temperatures, similar to the low-plasticity silt. The low-plasticity clay also achieved a lower temperature than the low-plasticity silt. For the low-plasticity clay, the OMC and the OMC + free water tests had samples with visually similar temperature profiles. Figure 4 shows the high-plasticity clay, which has notable differences from the previous soil types.

The frost penetrated deeper into the samples, and there was a sharper decrease when the thaw began. Figure 5 shows the poorly graded sand, which is classified as having a low-to-medium frost potential. There was minimal temperature change in these samples and minimal frost-depth penetration compared to the other soil types. The samples also had an increasing temperature profile over multiple cycles, compared to the generally decreasing profiles of previous soil types.

Figure 2. Frost-heave layer temperatures (T1 = top, T12 = bottom) for soil type ML. *Top*, optimum moisture content; *middle*, 10% lower than optimum moisture content; *bottom*, optimum moisture content with free water added. The horizontal axis is time in hours. The vertical axis is layer temperature in degrees Fahrenheit. The anomaly in the middle graph at approximately 72 hours was an unexpected power outage.
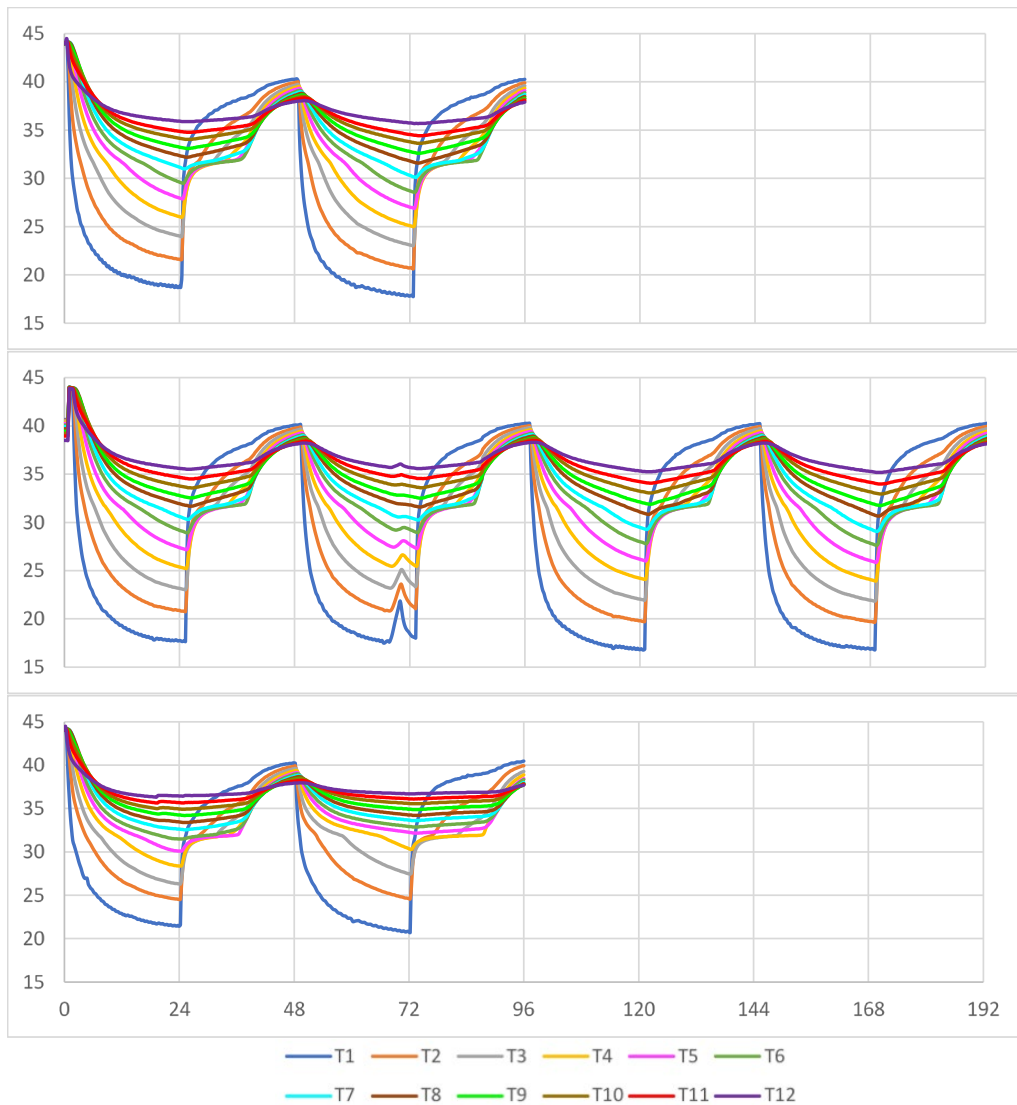
Figure 3. Frost-heave layer temperatures (T1 = top, T12 = bottom) for soil type CL. *Top*, optimum moisture content; *middle*, 10% lower than optimum moisture content; *bottom*, optimum moisture content with free water added. The horizontal axis is time in hours. The vertical axis is layer temperature in degrees Fahrenheit. The anomaly in the bottom graph at approximately 72 hours was an unexpected power outage.
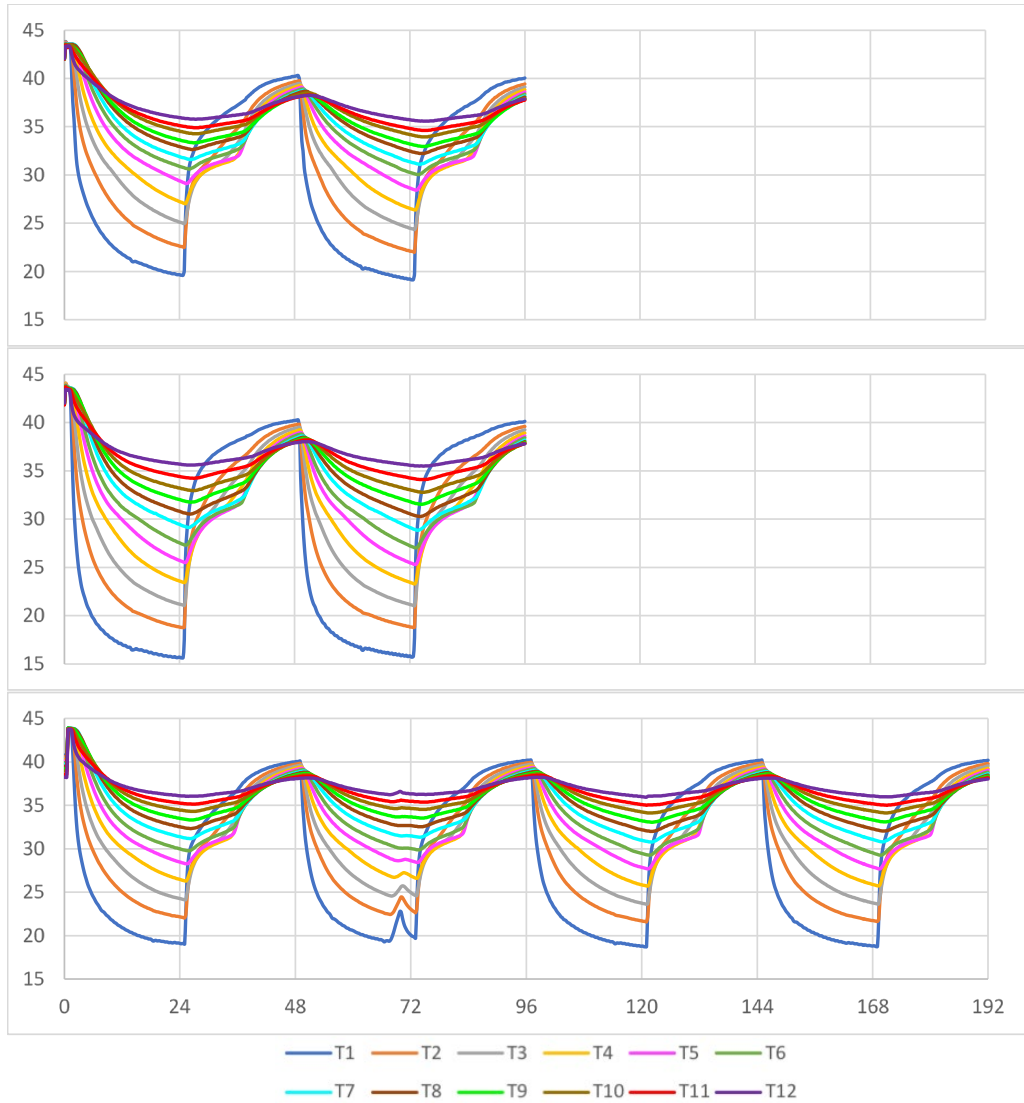
Figure 4. Frost-heave layer temperatures (T1 = top, T12 = bottom) for soil type CH. *Top*, optimum moisture content; *middle*, 10% lower than optimum moisture content; *bottom*, optimum moisture content with free water added. The horizontal axis is time in hours. The vertical axis is layer temperature in degrees Fahrenheit.
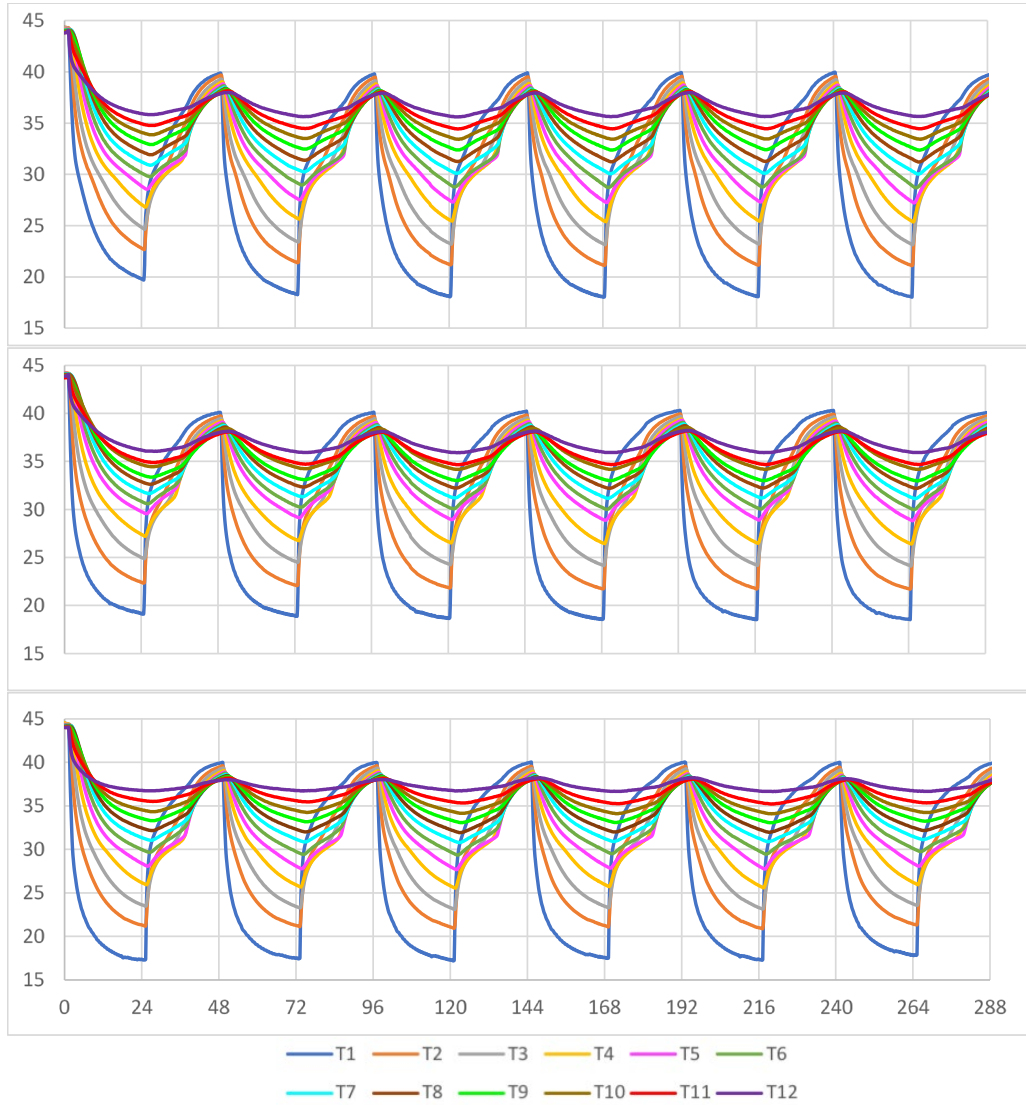
Figure 5. Frost-heave layer temperatures (T1 = top, T12 = bottom) for soil type SP. *Top*, optimum moisture content; *middle*, 10% lower than optimum moisture content; *bottom*, optimum moisture content with free water added. The horizontal axis is time in hours. The vertical axis is layer temperature in degrees Fahrenheit. The anomaly in the middle and bottom graphs at approximately 164 hours was an unexpected power outage.
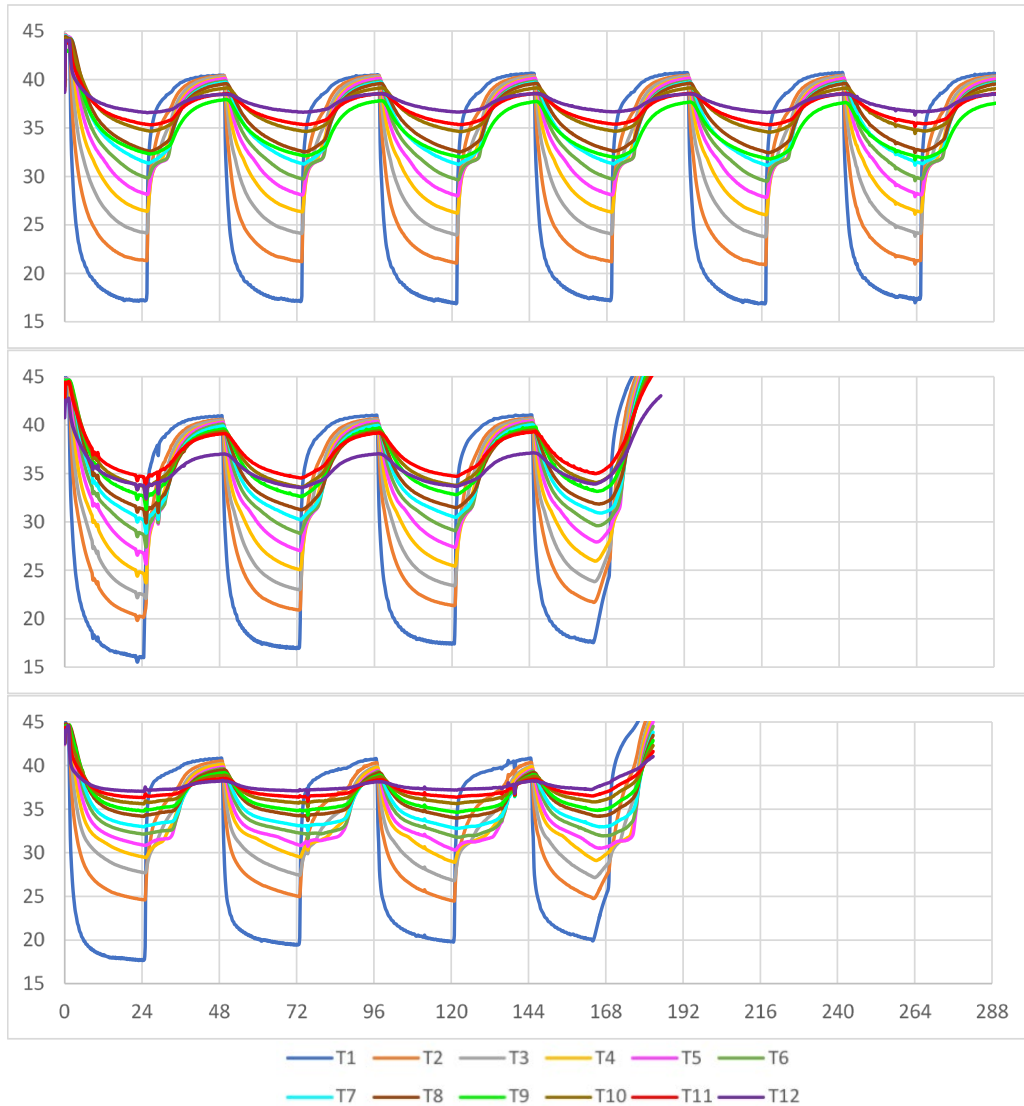
3.2 Mechanical properties of soils

As stated before, we characterized the soil properties through the tests listed in Table 2. The following sections discuss the soil's mechanical properties.

3.2.1 Moisture-density curves

We determined the OMC and maximum density by using the modified proctor test, ASTM D1557 (2012). Table 3 summarizes the results, which were used when creating later samples. Appendix A provides the full moisture-

density results. The amount of water needed for the sample size was calculated, and the soil was mixed and compacted to the appropriate volume to achieve the OMC and maximum density. The intent of the OMC – 10% material tests was to simulate a material with a lower density. It was difficult to determine the optimum moisture content for poorly graded sand, so the value selected was a lower water content than the theoretical optimum but was the highest density achieved.

Table 3. Moisture-density-curve results.

Soil Type	SP	ML	CL	CH
OMC (%)	3	7.8	10.8	15.6
Maximum density (lb/ft³)	113	131.9	128.2	114
OMC − 10% (%)	2.7	6.5	9.2	14
Maximum density − 10% (lb/ft³)	112	130	124	112

3.2.2 Particle size analysis

We performed a complete gradation on the samples by using ASTM D7928 (2017b). The gradations were then used to classify the materials according to the Unified Soil Classification Scheme. This ensured that the materials fell into the categories selected. Appendix A provides the gradations for each material.

3.2.3 Atterberg limits

The soil type's Atterberg limits, such as the liquid limit and plastic limit, were determined according to ASTM D4318 (2017a). The Atterberg limits test was used to identify the soil's plasticity index, liquid limit, and plastic limit. Table 4 summarizes the results of the Atterberg tests.

Table 4. Atterberg limits of the soils types tested. NR materials were noncohesive; NP materials had inconclusive testing

Soil Type	SP	ML	CL	CH
Liquid Limit	NR	20	23	71
Plastic Limit	NR	NP	17	21
Plasticity Index	NR	NP	6	50

3.3   Soil thermal conductivity versus time

Due to water having a higher thermal conductivity than dry soil, we expected the thermal conductivity to increase as the moisture content increased and number of freezing cycles increased, due to moisture migration

to the freezing front. We also expected frozen soil to have a higher thermal conductivity than thawed soil due to pure ice having a higher thermal conductivity compared to pure water. Figure 6 represents the ML soil's thermal conductivity results. In the ML soil type's OMC test, thermal conductivity increased slightly in the upper levels of the sample with successive freezing, with the exception of the second layer of the sample. We thought this to be due to the moisture migration caused by the sample undergoing sequential freezing and thawing, drawing moisture to the upper levels. When the sample thaws totally, the moisture eventually returns to equilibrium in the sample. The OMC – 10% moisture remained virtually unchanged except in the uppermost layers. The samples with free moisture available achieved the largest increase in thermal conductivity, and the increase continued with successive freezing cycles. The free-water condition has the most potential for moisture migration to the freezing front. In the extreme case, the increase was over six times the original value of thermal conductivity.

Figure 7 illustrates the low-plasticity clay and displays similar conductivity as the ML material. The OMC test's thermal conductivity increased slightly in the upper levels that were the coldest and experienced the largest moisture migration, similar to ML's OMC test. The OMC – 10% moisture condition exhibited slight increases in the upper levels, and the free-water condition showed the largest increase in the upper levels. The increase in thermal conductivity is not as large as for the ML material, but there is also lower moisture migration potential.

The high-plasticity clay in Figure 8 illustrates a similar increasing trend in the OMC sample's thermal conductivity. The OMC – 10% condition exhibited decreasing thermal conductivity in at the uppermost layers. At the T4 (4.2 in.) depth, the sample's thermal conductivity increased slightly. The high-plasticity clay had the lowest potential for moisture migration, and the T4 level may be where the moisture migrated to. The OMC – 10% test showed a trend similar to the OMC test, having sequential increases down to the 4.2 in. depth, only on a smaller scale.

The poorly graded silty sand in Figure 9 illustrates a surprisingly predictable change in thermal conductivity across multiple cycles. This trend is most visible in the OMC and OMC – 10% conditions. Assuming the change in thermal properties in those conditions is an effect of water freezing, then the deepest the frost penetrates is layer T8, or a depth of 9 in. In Fig-

ure 5, we see that T8 nears the freezing point of 32°F, suggesting the assumption may not be completely true, as we see that the thermal conductivity actually lowers during freezing, implying that the dominant effect is instead water content increase. In the OMD + free water case, these effects are obscured by the water content increase caused by the free-water source. The effect of water freezing still exists although it is only significant in the first two layers (1.8 in.). The layers most effected by the free-water source, T11 and T12, seem to plateau in value as water is added, rising to a large value. Although, these layers never froze, so it is unclear if they would have been affected.

Figure 6. Frost-heave layer conductivities (T1 = top, T12 = bottom) for soil type ML. *Top*, optimum moisture content; *middle*, 10% lower than optimum moisture content; *bottom*, optimum moisture content with free water added. The horizontal axis is time in hours. The vertical axis is layer conductivity in Btu/(hr*ft*°F).
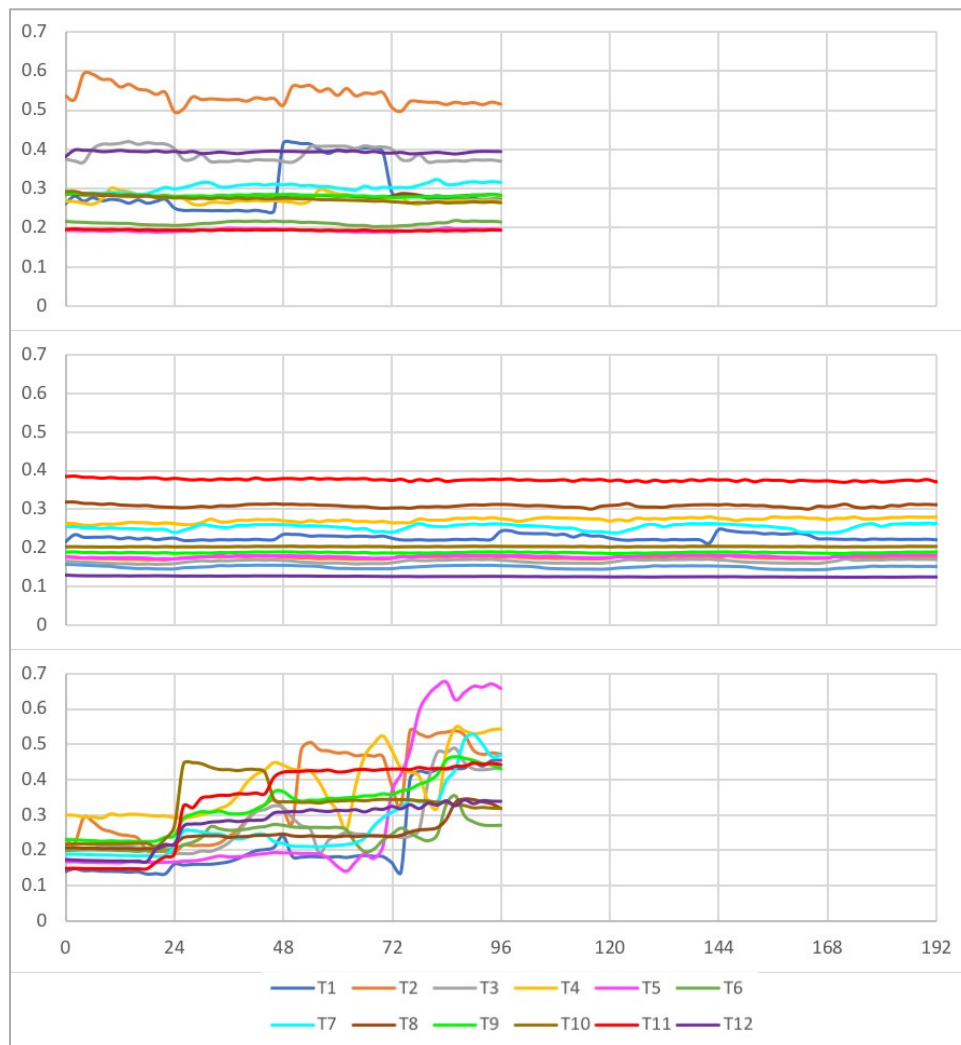
Figure 7. Frost-heave layer conductivities (T1 = top, T12 = bottom) for soil type CL. *Top*, optimum moisture content; *middle*, 10% lower than optimum moisture content; *bottom*, optimum moisture content with free water added. The horizontal axis is time in hours. The vertical axis is layer conductivity in degrees Fahrenheit.
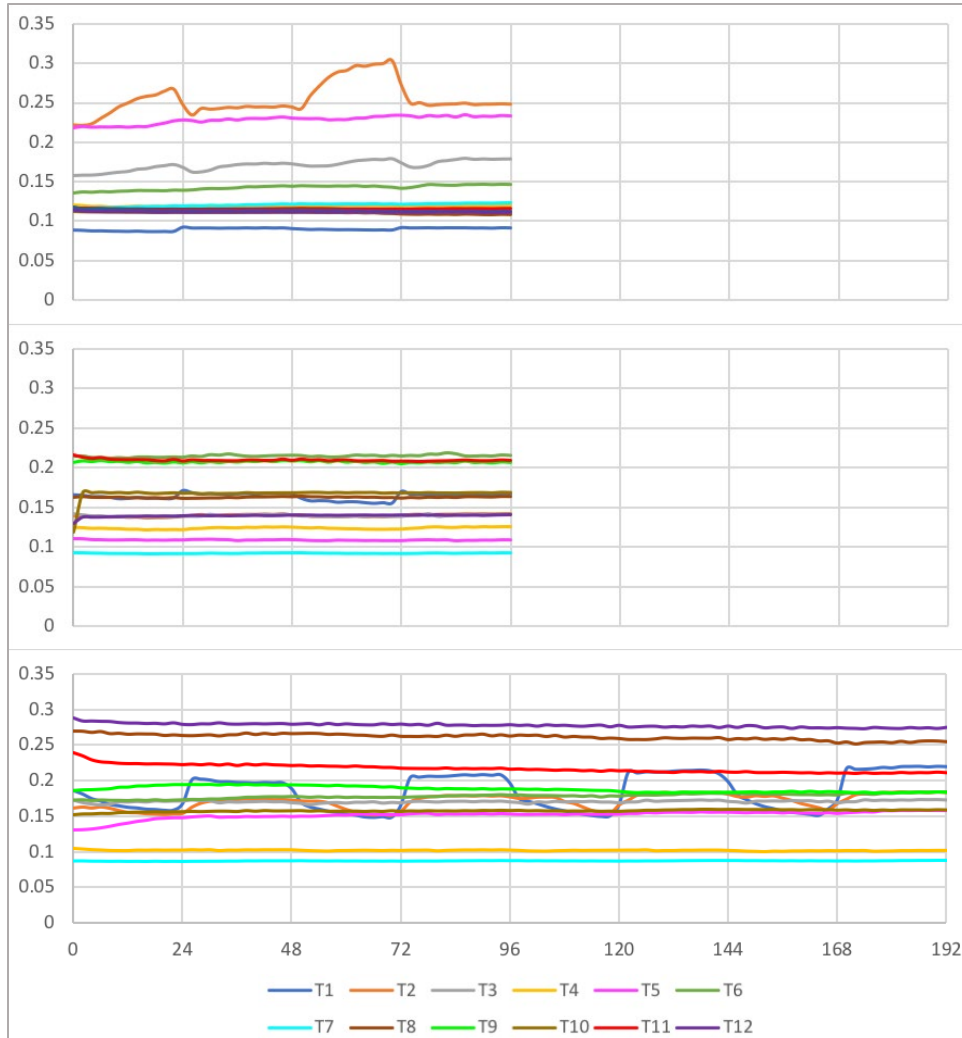
Figure 8. Frost-heave layer conductivities (T1 = top, T12 = bottom) for soil type CH. *Top*, optimum moisture content; *middle*, 10% lower than optimum moisture content; *bottom*, optimum moisture content with free water added. The horizontal axis is time in hours. The vertical axis is layer conductivity in Btu/(hr*ft*°F).
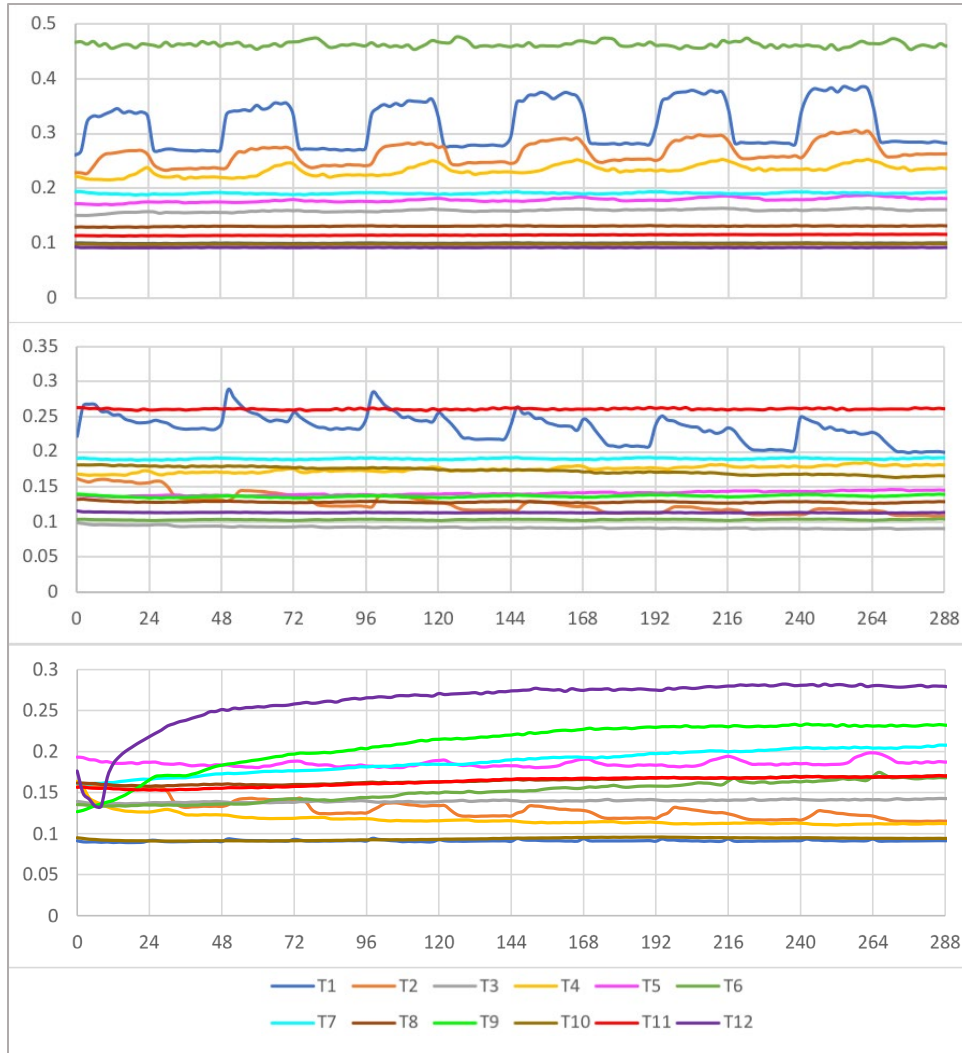
Figure 9. Frost-heave layer conductivities (T1 = top, T12 = bottom) for soil type SP. *Top*, optimum moisture content; *middle*, 10% lower than optimum moisture content; *bottom*, optimum moisture content with free water added. The horizontal axis is time in hours. The vertical axis is layer conductivity in in Btu/(hr*ft*°F).
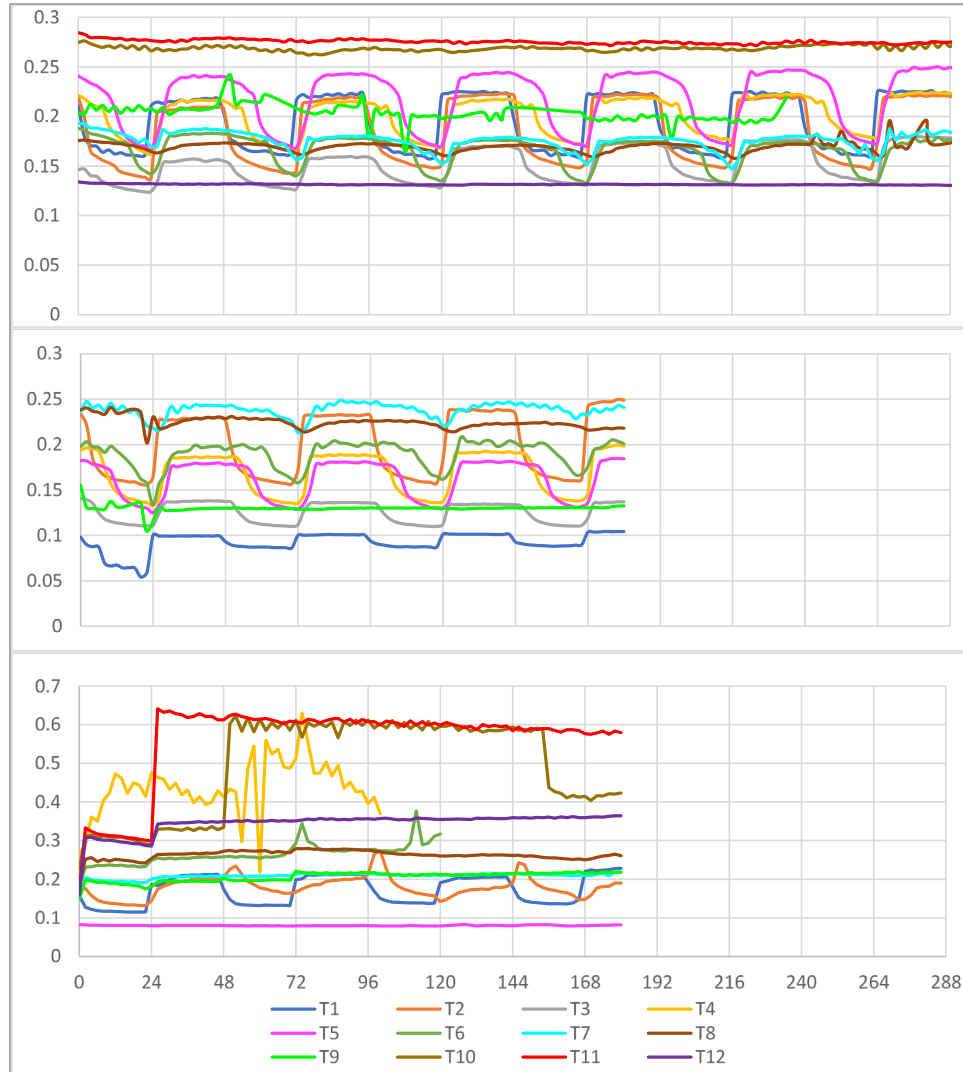
3.4   Moisture estimation

While there were no moisture probes in the samples during the frost-heave experiments, it was possible to record the final moisture contents by using the moisture recording method described in Section 2.2. We also found that this final moisture could be determined as a function of depth by separating the frost-heave samples into sections. Moisture intake over time was also calculated for the free-water results. Table 5 shows the final moisture contents for the samples.

Table 5. Final moisture contents for all soil types. *Top*, *middle*, and *bottom* correspond to the associated third of the sample used for moisture content measurement. For the ML soil type, the OMC and OMC + free water tests both had their bulk moisture contents taken. NA indicates missing results due to measurement failure. Included in final moisture for OMC + free water are moisture intakes due to the free-water source. Bulk moisture content increase associated with free water for ML, CL, CH, and SP are 3.72, 2.62, 1.11, and 5.90, respectively.

Moisture	OMC				OMC − 10%				OMC + Free Water			
Soil Type	ML	CL	CH	SP	ML	CL	CH	SP	ML	CL	CH	SP
Initial	7.80	9.20	15.60	3.00	6.50	9.20	14.00	2.70	7.80	10.80	15.60	3.00
Top		NA	15.15	NA	6.60	NA	15.15	2.69		11.65	NA	8.61
Middle	5.40	NA	14.90	NA	6.20	NA	14.90	2.56	12.7	12.05	NA	14.13
Bottom		NA	14.95	NA	6.00	NA	14.95	2.69		13.15	NA	14.34

As seen in the OMC and OMC − 10% results, there is a clear gradient of increasing moisture content with rising depth for CH and ML, while there is no clear indication for SP that a gradient exists, only that the middle layer has less water than the top or bottom third. This is logical as the increasing gradient upwards implies that the freezing front, which occurred predominantly in the top third of the sample for all soil types, was absorbing moisture and driving moisture migration upward. As the freezing front is in this region, moisture would be most converted to ice in these areas, which along with the resulting porosity change would pull moisture up from the lower layers due to capillary action. In the OMC + free water results, we see the opposite, a downward gradient; but in all cases, the moisture content is higher than the initial. This is also logical as the additional water will flow upwards, both through its own capillary action and to address the lowering moisture content in the above layers. The moisture flow from free water, as clearly shown, dominates in these cases, being a much more significant change compared to the capillary action of frost growth. From these estimates, we can see that moisture flow is a significant consequence of freezing and thawing of soils. As the local moisture content affects thermal properties, this moisture flow must be taken into account to improve frost-depth prediction accuracy. In future studies on this subject, we recommend incorporating in situ measurement of moisture content to more readily understand its role in frost action.

3.5   Frost heave and frost depth versus time

Figures 10 through 13 present the frost-heave and frost-depth penetration in a format similar to the ASTM for frost heave. There are separate scales on the frost-heave graphs because the samples with less water heaved less.

In all cases, when the material started to cool before freezing, there was a consolidation or slight decrease in frost heave.

Figure 10 shows that the frost heave for the ML material at OMC and OMC – 10% condition was minimal with a maximum of around 0.005 in. The frost did penetrate deeper in those samples. The sample with the free water available increased in frost-heave amount with successive frost cycles while the frost depth penetrated less.

Figure 10. Frost depth and heave for soil type ML for all three moisture conditions.
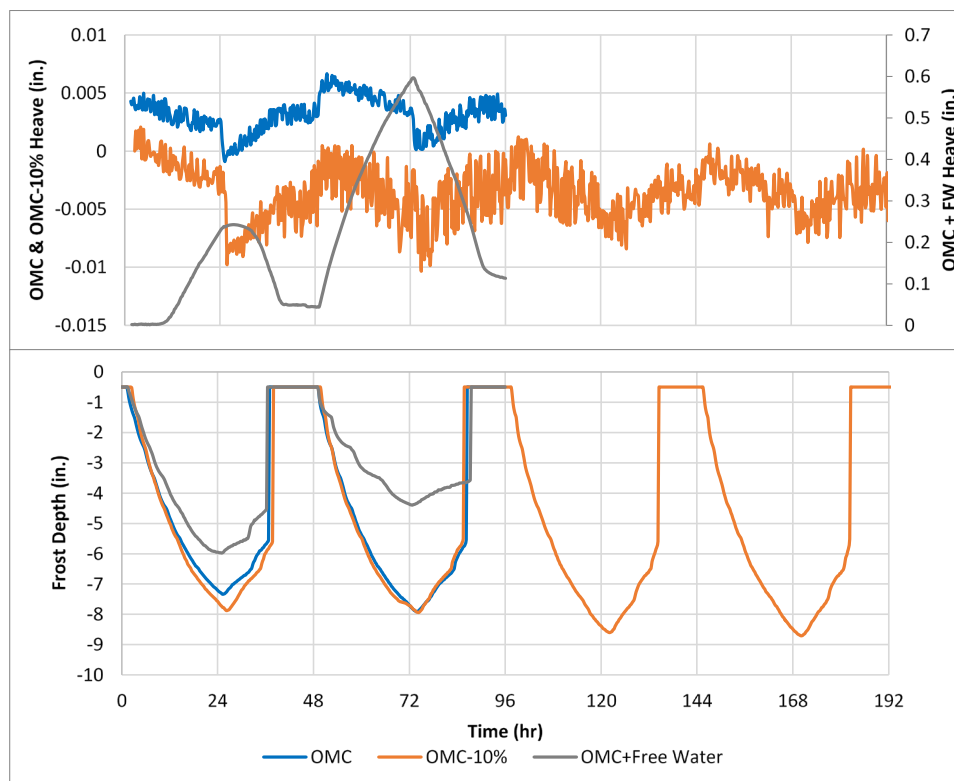
The low-plasticity clay in Figure 11 showed a deeper frost penetration in the material with less moisture while the OMC and OMC + free water were similar. Again, the samples with free water available exhibited an increase in frost heave; however, the heave amounts were minimal for all the CL material.

Figure 11. Frost depth and heave for soil type CL for all three moisture conditions.
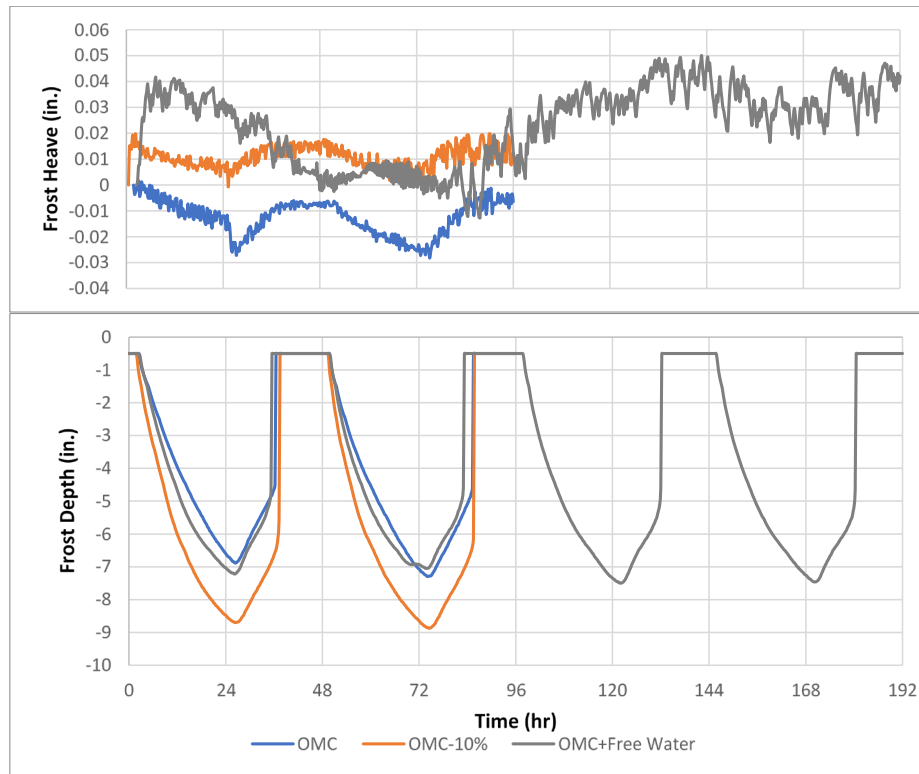
Figure 12 illustrates that the CH material at OMC froze about an inch deeper than in the OMC – 10% condition. The penetration trend for both materials increased as frost cycles continue. There is also a marked relaxation period, which appeared to remain constant at the low point and increased with frost cycles at the high point of the frost heave.

In Figure 13, we see that the SP material can freeze and heave even though it is considered to have medium frost susceptibility. In the OMC condition, we see not necessarily the most intense frost heave among all soil types but certainly the clearest indication of multiple frost cycles having an effect on frost heave and that this effect eventually reaches a maximum point after multiple cycles. We do not see this effect in the OMC – 10% condition, however, and due to sensor failure do not have an OMC + free water condition to compare. The maximum frost depth at each cycle shows a clear dependence on the moisture content, with higher moisture content conditions producing smaller maximum depths.

Figure 12. Frost depth and heave for soil type CH for all three moisture conditions.
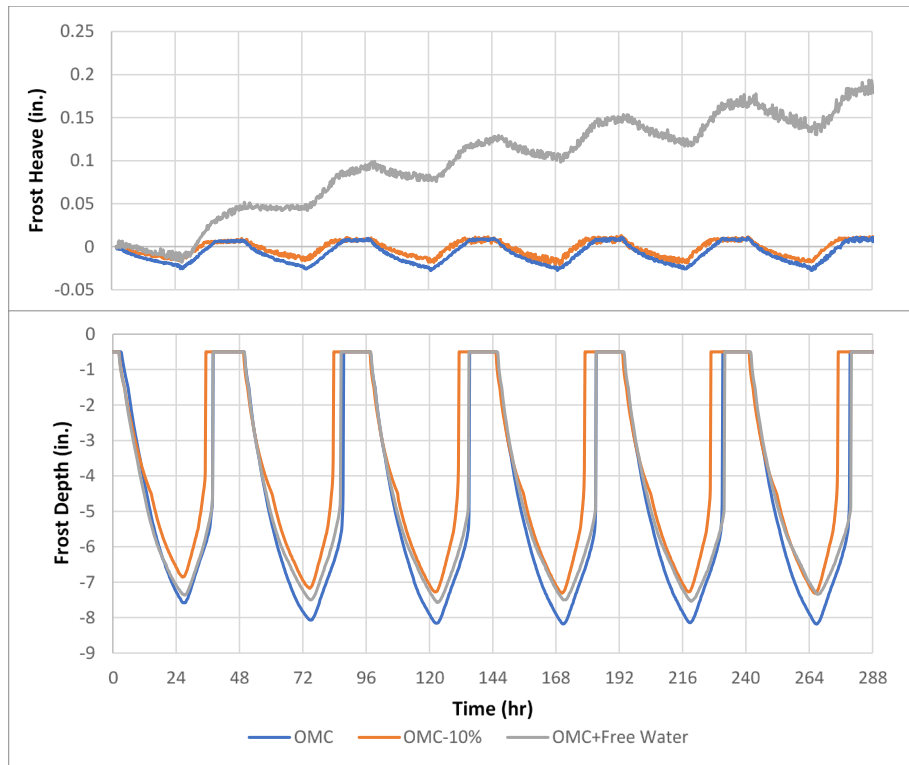
Figure 13. Frost depth and heave for soil type SP for all three moisture conditions. Frost heave is missing in OMC + free water due to sensor failure.
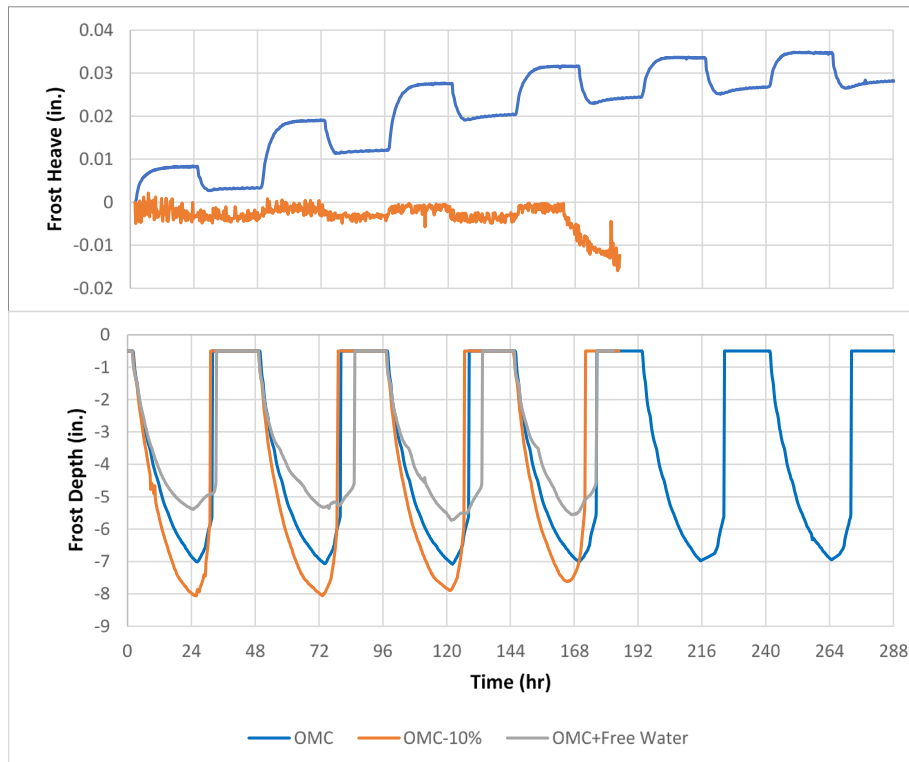
4 Model Development

4.1 Theory and derivation

To accurately predict frost depth and heave, our model must be able to accurately predict the change in temperature of the soil as a function of depth, time, and composition. It is this last factor that will significantly affect the competency of the model overall. Some of the main errors of the ModBerg equation, as discussed in section 1.1.2, are its assumptions about the frozen- and thaw-state values of thermal properties, such as thermal diffusivity and specific heat, and how the ratios of those properties interact. These assumptions lead to the inaccuracies ModBerg is known for, which can be seen in Table 6 where we compare our experimental results for soil thermal conductivity with those produced by ModBerg's constituent equations.

Table 6. Comparison of experimental results and ModBerg predictions for frozen and thawed soil thermal conductivity. Experimental thermal conductivity is the average value in the first four layers of the sample over the course of all frost or thaw periods.

Soil Classification	Moisture Content (%)	Max Density (lb/ft³)	Thermal Conductivity (Btu/hr*ft*°F)			
			Experimental Results		ModBerg Predictions	
			Frozen	Thawed	Frozen	Thawed
ML	OMC (7.8)	132	0.357	0.301	1.29	1.06
	−10% (6.5)	132	0.212	0.205	1.19	0.94
	OMC + Free Water (7.8)	132	0.291	0.23	1.29	1.06
CL	OMC (10.8)	128	0.176	0.165	1.35	1.18
	−10% (9.2)	128	0.132	0.134	1.23	1.08
	OMC + Free Water (10.8)	128	0.214	0.237	1.35	1.18
CH	OMC (15.6)	114	0.186	0.176	1.17	1.02
	−10% (14.0)	114	0.168	0.162	1.07	0.97
	OMC + Free Water (15.6)	114	0.146	0.144	1.17	1.02
SP	OMC (3.0)	113	0.168	0.196	0.54	0.83
	−10% (2.7)	113	0.152	0.189	0.37	0.59
	OMC + Free Water (3.0)	113	0.161	0.196	0.54	0.83

As the table shows, ModBerg's predictions do not match our experimental results and in all cases overestimate the thermal conductivity, producing

results much higher than intended. These differences are also not consistent for the thawed and frozen cases for each soil type, leading to errors in the ratios commonly seen in the ModBerg formula's correction factor.

As the major issues with ModBerg are its overestimation of properties and relationships, we will start our model with the pure energy balance equation, shown in equation (2).

$$\int_V \rho \dot{U} dV = \int_S q \, dS + \int_V r \, dV, \tag{2}$$

where

V = the volume,
S = the surface,
$\dot{U}$ = the time rate of internal energy,
q = the heat flux per unit area, and
r = the external heat source per unit volume.

The method that the ABAQUS FEM software uses is based on the above equation and determines the internal energy change based on uncoupled heat transfer (Dassault Systèmes 2018). Using this method, we can fully define the thermal systems based on only two parameters: thermal conductivity and specific heat. The original derivation of these parameters assumes them to be constant.

However, thermal conductivity and volumetric heat capacity cannot be taken as constants. These thermal parameters change with the current composition of the soil structure, just as moisture content, ice content, porosity, and the composition itself change with temperature. As the soil moisture freezes, the soil ice content increases while moisture and porosity decrease. To proceed, we must first identify the relationships between these thermal properties and composition and then the relationship between the contents and temperature. Equation (3) defines the relationship between conductivity and soil composition (Zhu 2006):

$$K = k_s^{\theta_s} * k_w^{\theta_w} * k_i^{\theta_i}, \tag{3}$$

where

$$K =$$ the effective thermal conductivity of the soil system,
$$k =$$ the thermal conductivity of the soil component,
$$\theta =$$ the component's volume fraction,
$$s =$$ soil,
$$w =$$ water, and
$$i =$$ ice.

In a similar fashion, volumetric heat capacity is treated as the sum of the fractional contributions of the soil components (Cengel and Boles 2018). This equation is defined as

$$C = \rho_s c_s \theta_s + \rho_w c_w \theta_w + \rho_i c_i \theta_i, \qquad (4)$$

where

$$C =$$ the volumetric heat capacity;
$$\rho =$$ the component density;
$$c =$$ the component specific heat capacity;
$$\theta =$$ the component's volume fraction; and, as before,
$$s =$$ soil,
$$w =$$ water, and
$$i =$$ ice.

With the two thermal parameters now defined in terms of the soil components, we can begin to replace some of the values with those known from literature. The thermal properties for water and ice are well known and will be considered constants in our model. The soil component conductivity was determined from earlier experimentation, and the soil specific heat will be taken from literature, namely the value used in the PCASE program for moist soils, which is a constant of 0.17 Btu/lb (Bianchini and Gonzalez 2012).

The only unknowns left in these equations are the volume fractions of the components, but the relationships between these values are known as are their initial values. The relationships between these are $1 = \theta_s + \theta_w + \theta_i + \theta_v$, $\theta_s = 1 - n$, and $n = \theta_w + \theta_i + \theta_v$, where n is the soil porosity and θ_v is the void fraction. θ_v, by definition, does not contribute to the above thermal properties. Initially, we assume the soil to contain no ice, allowing us to define all initial volume fractions and thus all initial thermal parameters from only the following parameters: soil volume fraction, thermal conductivity,

specific heat, water volume fraction (also known as moisture content), and porosity. All of these properties depend on the chosen soil type and location.

However, this is only valid for the initial soil conditions. As the soil freezes, moisture will convert into ice, and the soil will freeze. To determine the ice content, we must first determine the instantaneous moisture content, which also depends on temperature. The equation we will use to define this relationship is

$$\theta_{w_{new}} = \theta_w^* + \left(\theta_{w,initial} - \theta_w^*\right)e^{(T-T_0)/\alpha}, \tag{5}$$

where

$\theta_{w_{new}}$ = the instantaneous moisture content;
θ_w^* = the moisture content at a low reference temperature where ice content change is negligible;
$\theta_{w,initial}$ = the initial moisture content of the soil before it undergoes freezing;
T_0 = the soil freezing temperature (32°, by definition); and
α = the transition rate, a constant set at 11.26°F (Fukuda et al. 1997).

With the new moisture content, we are able to identify the ice content based on the previous relationships between volume fractions.

From these interactions, we are now able to depend on several material parameters and properties, some of which have been previously identified in literature, and some were determined experimentally in Section 3. There are, however, two critical assumptions to this model that must be made apparent. The first is a limit of ABAQUS FEM that internal moisture content must be held constant, which means that there is no modelling of moisture flow through the soil (Dassault Systèmes 2018). The second is that porosity change as a product of ice formation has not been introduced, meaning porosity is a constant. Due to these assumptions, the model will invariably have issues when any of three specific conditions are met: when soils are unsaturated, when significant or long-term moisture migration is relevant, and when porosity deviates from its initial value for a region over time. However, these factors will be considered in the later phases of model development. As our model gradually deviates from the ABAQUS FEM architecture, the first and second condition will be addressed. The third condition will be addressed as further experimentation

occurs, clarifying the role porosity has on the frost depth and the effect freeze–thaw cycles have on porosity.

4.2   Model results

Using equations (2) through (5) and the ABAQUS FEM software, we developed the Frost Response Of Soils at all Temperatures (FROST) model, shown at different stages of freeze–thaw (Figure 14). The inputs for this model were the moisture content, soil density, thermal conductivity, and soil specific heat, along with the same 24-hour freeze–thaw temperature schedule as in our experimental setup for frost heave. The models were simulated out to 96 hours each, and the frost depth was calculated from them using the same methods as for the experimental results. Figure 15 shows an updated version of the model with the capability for ice content prediction.

Figure 14. FROST model initial design at various stages.
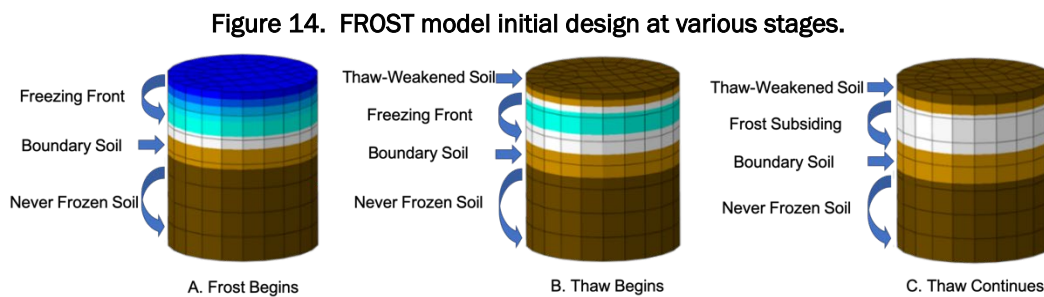
Figure 15. FROST model current design. *Left*, soil temperature in degrees Fahrenheit; *right*, ice/moisture content in volume fraction.
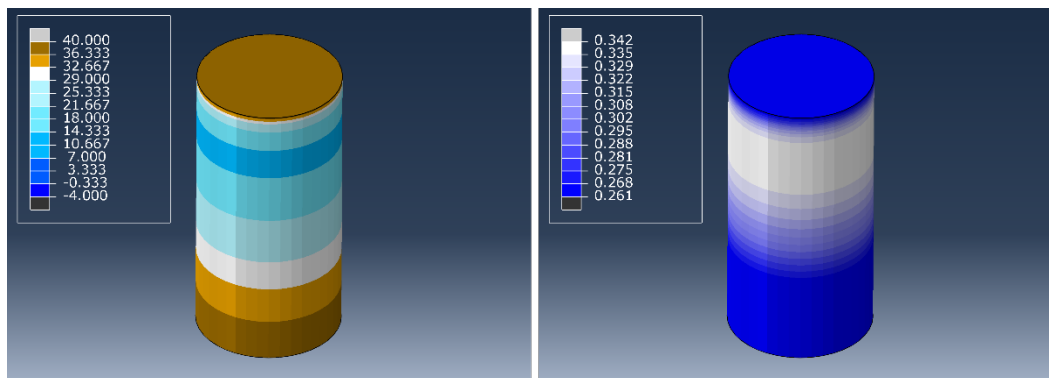
As shown in Figures 16–23, the FROST model is capable of predicting frost penetration depth for varying soil types and moisture contents; but there are clear visual differences between the predictions for the various soil types. The largest errors are in the thaw periods of the frost cycles (24–48 hours and 48–96 hours).

The OMC + free water experiments were not compared directly to the FROST model. As the FROST model does not yet have the ability to model moisture flow accurately, it is unable to accurately represent the frost-depth curves seen in the free-water experimental data. ModBerg is incapable of this analysis, also (Aldrich and Paynter 1953). For these reasons, we will not compare the FROST model to the free-water results.

The shape of the freeze–thaw cycle curves of the test samples showed similarities to the model. However, there are changes in the experimental cycle curves from cycle to cycle that do not occur in the model, such as with Figure 16's change between the first and second cycle. This is likely due to the model not yet integrating porosity and moisture-flow changes, which would change the model's state over multiple cycles.

Figure 16. Comparisons between experimental results for soil type ML at OMC and the FROST model.

Figure 17. Comparisons between experimental results for soil type CL at OMC and the FROST model. Only the first two freeze–thaw cycles are shown.

Figure 18. Comparisons between experimental results for soil type CH at OMC and the FROST model. Only the first two freeze–thaw cycles are shown.

Figure 19. Comparisons between experimental results for soil type SP at OMC and the FROST model. Only the first two freeze–thaw cycles are shown.

Figure 20. Comparisons between experimental results for soil type ML at OMC − 10% and the FROST model. Only the first two freeze–thaw cycles are shown.

Figure 21. Comparisons between experimental results for soil type CL at OMC – 10% and the FROST model. Only the first two freeze–thaw cycles are shown.
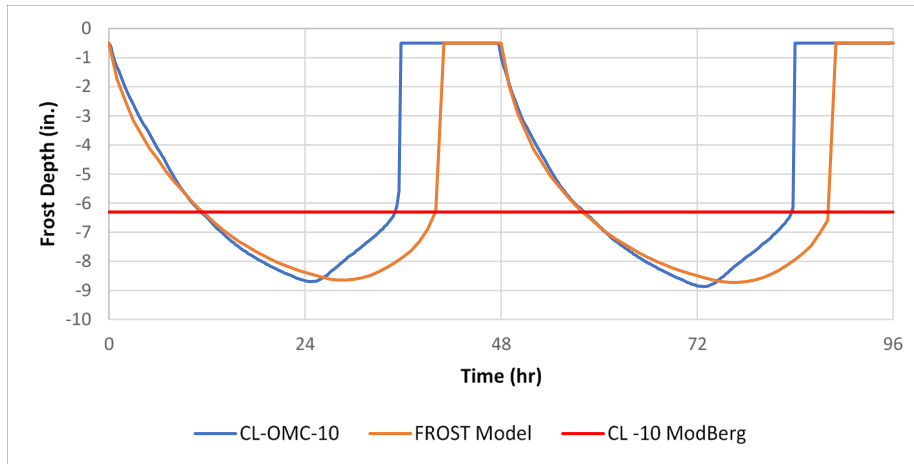
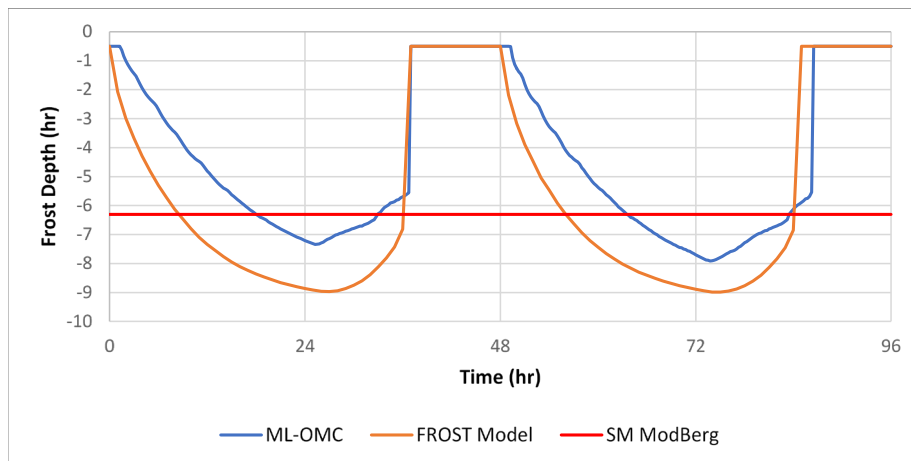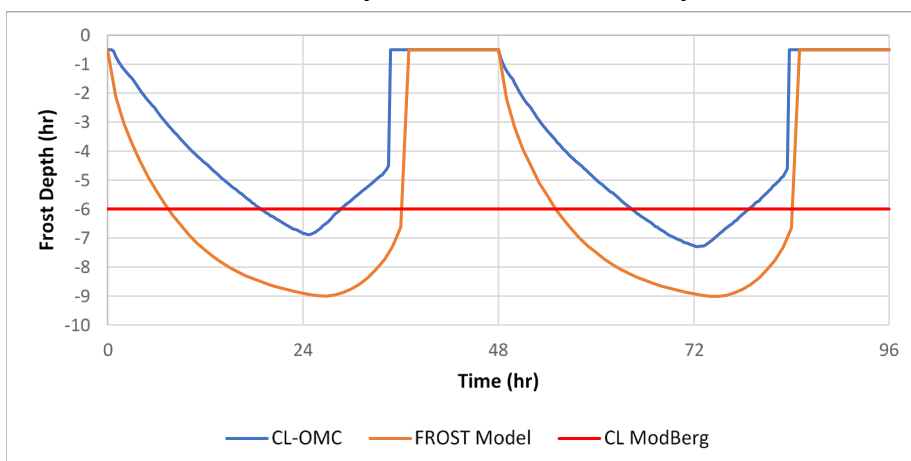Figure 22. Comparisons between experimental results for soil type CH at OMC – 10% and the FROST model. Only the first two freeze–thaw cycles are shown.
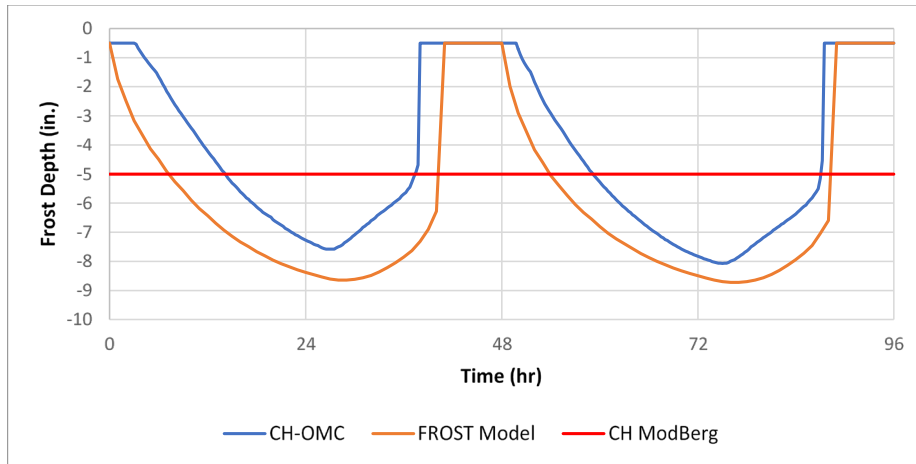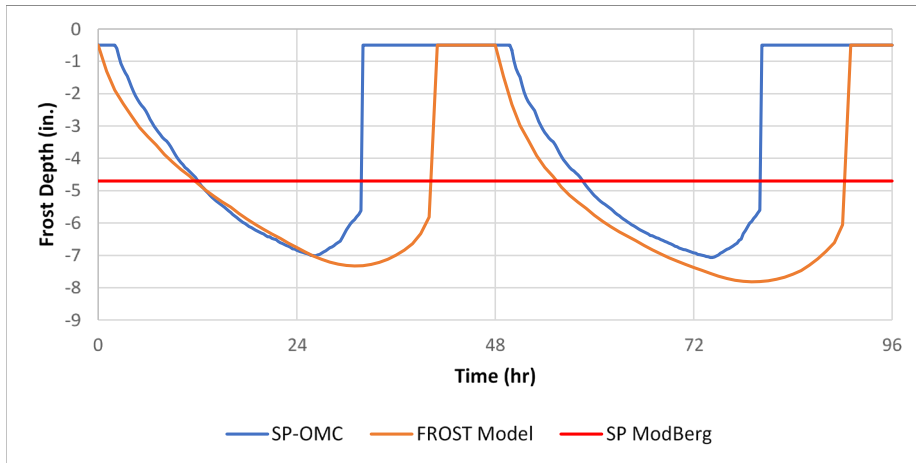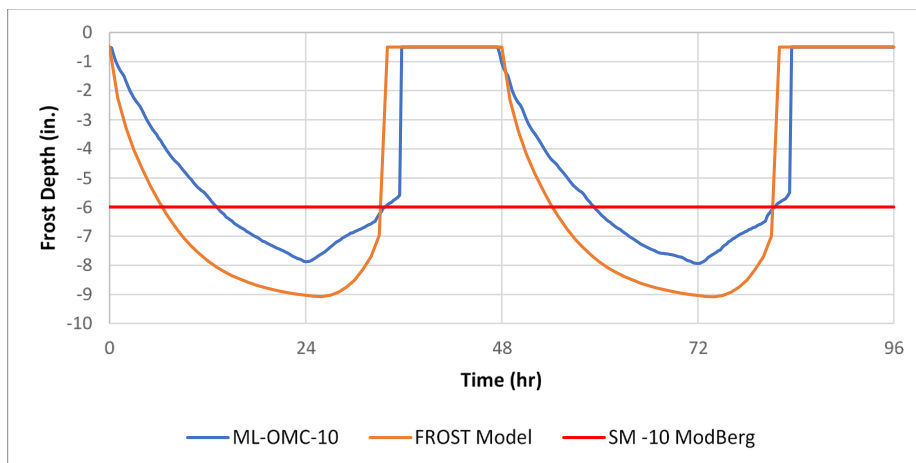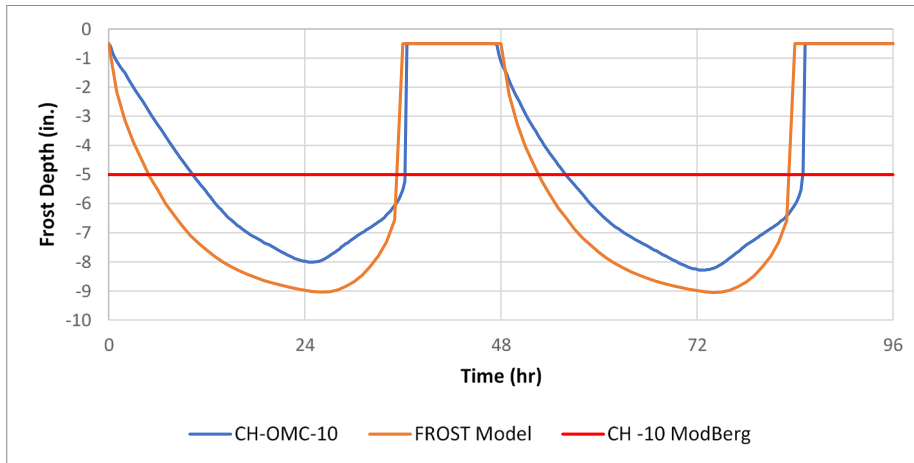

Figure 23. Comparisons between experimental results for soil type SP at OMC – 10% and the FROST model. Only the first two freeze–thaw cycles are shown.
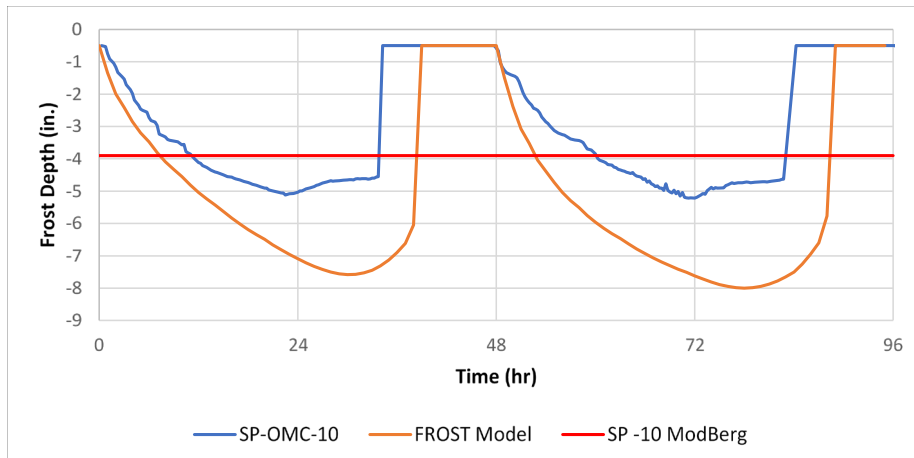
4.3   Model capabilities and limitations

As shown in Figures 16–23, the model makes a general approximation of the frost depth but has issues predicting the frost penetration rate and maximum frost depth, although the reasons can be readily be explained. Moisture flow would be more significant during the thaw state than the freezing states. However, moisture flow is not negligible during the thaw state, leading to issues in accuracy. Overall, the models overpredict depth, implying the moisture flow is crucial in this regard. This interaction is valid due to the higher heat capacity and lower thermal conductivity of water compared to soils, leading to a lower thermal diffusivity as the water content increases. Table 7 demonstrates this by comparing frost penetration depth between the experiment, the ModBerg equation, and the FROST model. It also compares the variance of the FROST model curve fit to experimental data.

Table 7. Comparisons of frost depth between experimental, calculated, and model results for OMC and OMC − 10% conditions. Variance is over the full 96 hours.

Soil Type	Moisture Content	Frost Depth (in.)			FROST Error (%)	ModBerg Error (%)	Variance
		Experiment	ModBerg	FROST			
ML	OMC (7.8)	7.63	6.3	8.98	18	17	1.85
ML	−10% (6.5)	7.91	6.0	9.08	15	24	1.45
CH	OMC (15.6)	7.82	5.0	8.72	11	36	1.63
CH	−10% (14.0)	8.15	5.0	9.05	11	39	1.22
CL	OMC (10.8)	7.09	6.0	9.01	27	15	1.99
CL	−10% (9.2)	8.79	6.3	8.72	1	28	1.82
SP	OMC (3.0)	7.04	4.7	7.82	11	33	2.48
SP	−10% (2.7)	5.38	3.9	8.00	49	28	2.66

In terms of frost-depth prediction, the FROST model has an average relative error of 18% across all tested soil types and moisture conditions, which for a frost depth of 8 in. is an error of about 1.4 in. Meanwhile, the ModBerg equation has an average relative error of 28%, which for the same frost depth of 8 in. is an error of about 2.2 in. Interestingly, ModBerg underpredicted the frost depth in all cases while the FROST model overpredicted in almost all cases. The FROST model was closer to the experimental frost depth when compared to ModBerg. This is expected as the FROST model incorporates changes in thermal properties as a function of ice and moisture content while ModBerg assumes these properties to be

constant, and the values it assumes to be constant are not in agreement with experiments.

Ultimately, the FROST model's capabilities are an improvement over Mod-Berg for the experimental tests but still requires improvements to its capabilities and additional testing. The next phase of the FROST model's development will focus on integrating moisture-flow capabilities, which currently are not possible with the ABAQUS framework (Dassault Systèmes 2018). As the moisture-flow capability is added in, we will compare the model to the current experimental results, future large-scale testing, and the previously omitted free-water tests. Once the model is capable of simulating moisture flow, porosity will also be implemented, allowing for a more accurate representation of moisture and permeability as the model goes through multiple freeze–thaw cycles.

5 Conclusions

The ongoing experimentation for the FROST model development has yielded more accurate results than ModBerg by taking into account the creation of ice layers within the frost depth. The completed experiments have created a more accurate prediction of frost-depth and heave potential. This information could be valuable in all earthen structures from roads to embankments to dams that are exposed to multiple freeze and thaw cycles.

The relationship between frost depth and temperature is affected by the amount of moisture available and the soil type, which is classified by particle sizes and liquid limits. The frost-heave tests showed that the thermal conductivity did not increase at all locations in each sample but was localized. We theorize that the thermal conductivity increased at depths within the samples where the moisture migration was concentrated, such as at the freezing front.

The frost-heave test results showed that the frost heave was greatest in the ML material with free water available. This makes sense as this material has the largest porosity and the largest void spaces, which support capillary action to drop in greater moisture to the freezing front. Frost heave and frost depth were the most diminished in the SP material, which is supported by its particle sizes being extremely large, inhibiting capillary action during freezing. The CL and CH materials behaved similarly, although CH was more uniform in its results and it seemed the least impacted by the free-water tests.

The FROST model was able to represent the general freezing curve with reasonable accuracy but had large errors during the thaw portion of the freeze–thaw cycle. Because of limitations on modelling moisture flow and porosity and due to the thaw portion being where these effects would be the most significant, this error is understandable. We should also point out that in all cases the FROST model overpredicted frost depth, while the ModBerg equation underpredicted it; yet on average, the FROST model was closer to the actual frost depth than not and was able to mimic its dependency on frost cycle, which the ModBerg equation is unable to calculate. The FROST model's primary focus for improvement in the future will be on addressing these current limitations, leading to a more accurate prediction of frost depth than achievable with traditional analytical equations.

References

Aldrich, H. P., Jr., and H. M. Paynter. 1953. *Analytical Studies of Freezing and Thawing of Soils*. Boston: Arctic Construction and Frost Effects Laboratory.

American Association of State Highway and Transportation Officials. 2008. *Mechanistic-Empirical Pavement Design Guide: A Manual of Practice*. Washington, DC: American Association of State Highway and Transportation Officials.

ASTM International. 2012. *Standard Test Methods for Laboratory Compaction Characteristics of Soil Using Modified Effort (56,000 ft-lbf/ft3 (2,700 kN-m/m3))*. ASTM D1557-12e1. West Conshohocken, PA: ASTM International. https://doi.org/10.1520/D1557-12E01.

———. 2013a. *Standard Practice for Using Significant Digits in Geotechnical Data*. ASTM D6026-13. West Conshohocken, PA: ASTM International. https://doi.org/10.1520/D6026-13.

———. 2013b. *Standard Test Methods for Frost Heave and Thaw Weakening Susceptibility of Soils*. ASTM D5918-13e1. West Conshohocken, PA: ASTM International. https://doi.org/10.1520/D5918-13E01.

———. 2014. *Standard Test Method for Determination of Thermal Conductivity of Soil and Soft Rock by Thermal Needle Probe Procedure*. ASTM D5334-14. West Conshohocken, PA: ASTM International. https://doi.org/10.1520/D5334-14.

———. 2015. *Standard Specification for Graded Aggregate Material for Bases or Subbases for Highways or Airports*. ASTM D2940/D2940M-15. West Conshohocken, PA: ASTM International. https://doi.org/10.1520/D2940_D2940M-15.

———. 2016. *Standard Test Method for California Bearing Ratio (CBR) of Laboratory-Compacted Soils*. ASTM D1883-16. West Conshohocken, PA: ASTM International. https://doi.org/10.1520/D1883-16.

———. 2017a. *Standard Test Methods for Liquid Limit, Plastic Limit, and Plasticity Index of Soils*. ASTM D4318-17e1. West Conshohocken, PA: ASTM International. https://doi.org/10.1520/D4318-17E01.

———. 2017b. *Standard Test Method for Particle-Size Distribution (Gradation) of Fine-Grained Soils Using the Sedimentation (Hydrometer) Analysis*. ASTM D7928-17. West Conshohocken, PA: ASTM International. https://doi.org/10.1520/D7928-17.

———. 2018. *Standard Test Method for Effective Porosity and Effective Air Voids of Compacted Asphalt Mixture Samples*. ASTM D7063/D7063M-18. West Conshohocken, PA: ASTM International. https://doi.org/10.1520/D7063_D7063M-18.

———. 2019. *Standard Test Methods for Laboratory Determination of Water (Moisture) Content of Soil and Rock by Mass*. ASTM D2216-19. West Conshohocken, PA: ASTM International. https://doi.org/10.1520/D2216-19.

Atkins, R. T., and E. A. Wright. 1990. *Thermistor-Based Thermal Conductivity Measurement System.* Special Report 90-24. Hanover, NH: U.S. Army Cold Regions Research and Engineering Laboratory.

Ban, H., S. Im, Y.-R. Kim, and J. S. Jung. 2017. "Laboratory Tests and Finite Element Simulations to Model Thermally Induced Reflective Cracking of Composite Pavements." *International Journal of Pavement Engineering* 19 (3): 220–230. https://doi.org/10.1080/10298436.2017.1279491.

Berg, R. L., G. L. Guymon, and T. C. Johnson. 1980. *Mathematical Model to Correlate Frost Heave of Pavements with Laboratory Predictions.* CRREL Report 80-10. Hanover, NH: U.S. Army Cold Regions Research and Engineering Laboratory.

Berg, R., and T. Johnson. 1983. *Revised Procedure for Pavement Design under Seasonal Frost Conditions.* Special Report 83-27. Hanover, NH: U.S. Army Cold Regions Research and Engineering Laboratory. http://hdl.handle.net/11681/11660.

Bianchini, A., and C. R. Gonzalez. 2012. *Pavement-Transportation Computer Assisted Structural Engineering (PCASE) Implementation of the Modified Berggren (ModBerg) Equation for Computing the Frost Penetration Depth within Pavement Structures.* ERDC/GSL TR-12-15. Vicksburg, MS: Engineer Research and Development Center. http://hdl.handle.net/11681/10399.

Bigl, S. R., and S. A. Shoop. 1994. *Soil Moisture Prediction During Freeze and Thaw Using a Coupled Heat and Moisture Flow Model.* CRREL Report 94-11. Hanover, NH: U.S. Army Cold Regions Research and Engineering Laboratory. http://hdl.handle.net/11681/9376.

Black, P. B. 1995. *RIGIDICE Model of Secondary Frost Heave.* CRREL Report 95-12. Hanover, NH: U.S. Army Cold Regions Research and Engineering Laboratory. http://hdl.handle.net/11681/9186.

Braley, W. A., and B. Connor. 1989. *Berg2: Micro-Computer Estimation of Freeze and Thaw Depths and Thaw Consolidation.* Fairbanks, AK: State of Alaska Department of Transportation and Public Facilities.

Cengel, Y. A., and M. A. Boles. 2018. *Thermodynamics: An Engineering Approach.* New York: McGraw-Hill Education.

Dassault Systèmes. 2018. *SIMULIA Abaqus User Assistance.* https://help.3ds.com.

Departments of the Army and the Air Force. 1988. *Arctic and Subarctic Construction Calculation Methods for Determination of Depths of Freeze and Thaw in Soils.* Washington, DC: Departments of the Army and the Air Force. https://www.wbdg.org/FFC/ARMYCOE/COETM/ARCHIVES/tm_5_852_6.pdf.

Fukuda, M., H. Kim, and Y. Kim. 1997. "Preliminary Results of Frost Heave Experiments Using Standard Test Sample Provided by TC8." In *Proceedings, International Symposium on Ground Freezing and Frost Action in Soils*, 15–17 April, Luleå, Sweden, ed. S. Knutsson. http://www5.unitn.it/Biblioteca/it/Web/EngibankFile/Ground%20freezing.pdf.

Guyer, J. P. 2013. *An Introduction to Pavement Design in Seasonal Frost Condtions.* El Macero, CA: Guyer Partners.

Guymon, G. L., R. L. Berg, and T. V. Hromadka. 1993. *Mathematical Model of Frost Heave and Thaw Settlement in Pavements*. Hanover, NH: U.S. Army Cold Regions Research and Engineering Laboratory.

Hammons, M. I. 1998. *Advanced Pavement Design: Finite Element Modeling for Rigid Pavement Joints, Report II: Model Development*. DOT/FAA/AR-97/7. Washington, DC: Office of Aviation Research. https://apps.dtic.mil/dtic/tr/fulltext/u2/a342915.pdf.

Holanda, A., L. Tadeu, B. De Melo, and J. B. Soares. 2006. "Finite Element Modeling of Flexible Pavements." In *Proceedings of the XXVII Iberian Latin-American Congress on Comptutational Methods in Engineering*, 3–6 September, Belém, Brazil, 27:1–14. http://repositorio.ufc.br/handle/riufc/1380.

Kim, M. 2007. *Three-Dimensional Finite Element Analysis of Flexible Pavements Considering Nonlinear Pavement Foundation Behavior*. Urbana, IL: University of Illinois at Urbana-Champaign.

Leonardi, G. 2014. "Finite Element Analysis of Airfield Flexible Pavement." *Archives of Civil Engineering* 60 (3): 323–334.

Rajaei, P., and G. Y. Baladi. 2015. "Frost Depth, General Prediction Model." *Transportation Research Record: Journal of the Transportation Research Board* 2510:74–80.

Shastri, A., and M. Sanchez. 2014. "Numerical Modeling of Frozen Soils." *Geo-Congress 2014*, 23–26 February, Atlanta, GA, 234:3476–3486. https://doi.org/10.1061/9780784413272.337.

Shoop, S., R. Affleck, V. C. Janoo, R. B. Haehnel, and B. Barrett. 2005. *Constitutive Model for a Thawing, Frost-Susceptible Sand*. ERDC/CRREL TR-05-3. Hanover, NH: U.S. Army Engineer Research and Development Center. http://hdl.handle.net/11681/5388.

Soil Engineering Division. 1957. *Frost Penetration in Multilayer Soil Profiles*. ACFEL TR-67. Boston: Arctic Construction and Frost Effects Laboratory. http://hdl.handle.net/11681/6587.

U.S. Army Corps of Engineers. 1984. *Pavement Criteria for Seasonal Frost Conditions*. EM 1110-3-138. Washington, DC: U.S. Army Corps of Engineers. https://www.publications.usace.army.mil/portals/76/publications/engineermanuals/em_1110-3-138.pdf.

Yassenn, O. M., I. R. Endut, S. Z. Ishak, M. A. Hafez, and H. M. Yaseen. 2015. "Finite Element Modeling of Flexible Pavement." *Journal of Multidisciplinary Engineering Science and Technology* 2 (1): 115–120.

Zarling, J. F., W. A. Braley, and C. Pelz. 1991. "The Modified Berggren Method—A Review." In *Cold Regions Engineering: Proceedings of the Fifth International Conference*, 262–273. Lebanon, NH: American Society of Civil Engineers.

Zhu, M. 2006. "Modeling and Simulation of Frost Heave in Frost-Susceptible Soils." PhD thesis, University of Michigan. http://hdl.handle.net/2027.42/125791.

Appendix A: Supplementary Figures

Figure A-1. Example particle size distribution chart for soil type ML

Figure A-2. Example Particle Size Distribution chart for soil type CL

Particle Size Distribution Report

% +3"	% Gravel		% Sand			% Fines	
	Coarse	Fine	Coarse	Medium	Fine	Silt	Clay
0.0	0.0	3.2	3.3	11.1	13.8	25.9	42.7

TEST RESULTS

Opening Size	Percent Finer	Spec.* (Percent)	Pass? (X=Fail)
.375	100.0		
#4	96.8		
#10	93.5		
#20	88.7		
#40	82.4		
#60	76.4		
#100	72.3		
#200	68.6		
0.0223 mm.	65.8		
0.0163 mm.	59.2		
0.0102 mm.	54.3		
0.0075 mm.	51.0		
0.0055 mm.	44.4		
0.0028 mm.	36.1		
0.0012 mm.	27.8		

* (no specification provided)

Material Description

FERF CLAY

Atterberg Limits (ASTM D 4318)
PL= 20   LL= 30   PI= 10

Classification
USCS (D 2487)= CL   AASHTO (M 145)= A-4(5)

Coefficients
D_{90}= 1.0255 D_{85}= 0.5458 D_{60}= 0.0170
D_{50}= 0.0071 D_{30}= 0.0015 D_{15}=
D_{10}= C_u= C_c=

Remarks

Date Received: _____   Date Tested: _____
Tested By: _____
Checked By: _____
Title: _____

Date Sampled:

US ARMY - CRREL

Hanover, New Hampshire

Client: Wade Lein
Project: PCASE frost depth Project

Project No: Figure

Figure A-3. Example Particle Size Distribution chart for soil type CH

Particle Size Distribution Report

% +3"	% Gravel		% Sand			% Fines	
	Coarse	Fine	Coarse	Medium	Fine	Silt	Clay
0.0	0.0	0.2	1.0	2.8	4.4	30.1	61.5

TEST RESULTS

Opening Size	Percent Finer	Spec.* (Percent)	Pass? (X=Fail)
3/4	100.0		
3/8	100.0		
#4	99.8		
#10	98.8		
0.0215 mm.	87.5		
0.0159 mm.	77.8		
0.0100 mm.	71.9		
0.0073 mm.	66.0		
0.0053 mm.	62.1		
0.0027 mm.	52.1		
0.0012 mm.	39.5		

* (no specification provided)

Material Description

Manufactured Soil

Atterberg Limits (ASTM D 4318)

PL= 21   LL= 71   PI= 50

Classification

USCS (D 2487)= CH   AASHTO (M 145)= A-7-6(51)

Coefficients

D_{90}= 0.0448 D_{85}= 0.0200 D_{60}= 0.0045
D_{50}= 0.0024 D_{30}= D_{15}=
D_{10}= C_u= C_c=

Remarks

Date Received: _____   Date Tested: 8/3/2018

Tested By: Allan Wheeler _____

Checked By: _____

Title: _____

Date Sampled:

US ARMY - CRREL

Hanover, New Hampshire

Client: Wade Lein
Project: Frost Model

Project No: Figure

Figure A-4. Example Particle Size Distribution chart for soil type SP

Particle Size Distribution Report

PERCENT FINER

GRAIN SIZE - mm.

% +3"	% Gravel		% Sand			% Fines	
	Coarse	Fine	Coarse	Medium	Fine	Silt	Clay
			10.2	39.9	46.2	3.3	

TEST RESULTS

Opening Size	Percent Finer	Spec.* (Percent)	Pass? (X=Fail)
#4	99.6		
#10	89.4		
#20	74.2		
#40	49.5		
#60	23.9		
#100	9.1		
#200	3.3		

* (no specification provided)

Material Description

Concrete Sand

Atterberg Limits (ASTM D 4318)

PL=   LL=   PI=

Classification

USCS (D 2487)= SP   AASHTO (M 145)=

Coefficients

D_{90}= 2.0877 D_{85}= 1.4571 D_{60}= 0.5438
D_{50}= 0.4296 D_{30}= 0.2866 D_{15}= 0.1942
D_{10}= 0.1578 C_u= 3.45 C_c= 0.96

Remarks

Date Received: _____ Date Tested: 8/1/2018

Tested By: Allan Wheeler

Checked By: _____

Title: _____

Date Sampled:

US ARMY - CRREL

Hanover, New Hampshire

Client: Wade Lein
Project: Frost Model

Project No: Figure

Figure A-5. Replicate frost-heave layer temperatures (T1 = top, T12 = bottom) for soil type ML. Top, optimum moisture content; middle, 10% lower than optimum moisture content; bottom, optimum moisture content with free water added. The horizontal axis is time in hours. The vertical axis is layer temperature in degrees Fahrenheit. The anomaly in the middle graph at approximately 72 hours was an unexpected power outage.
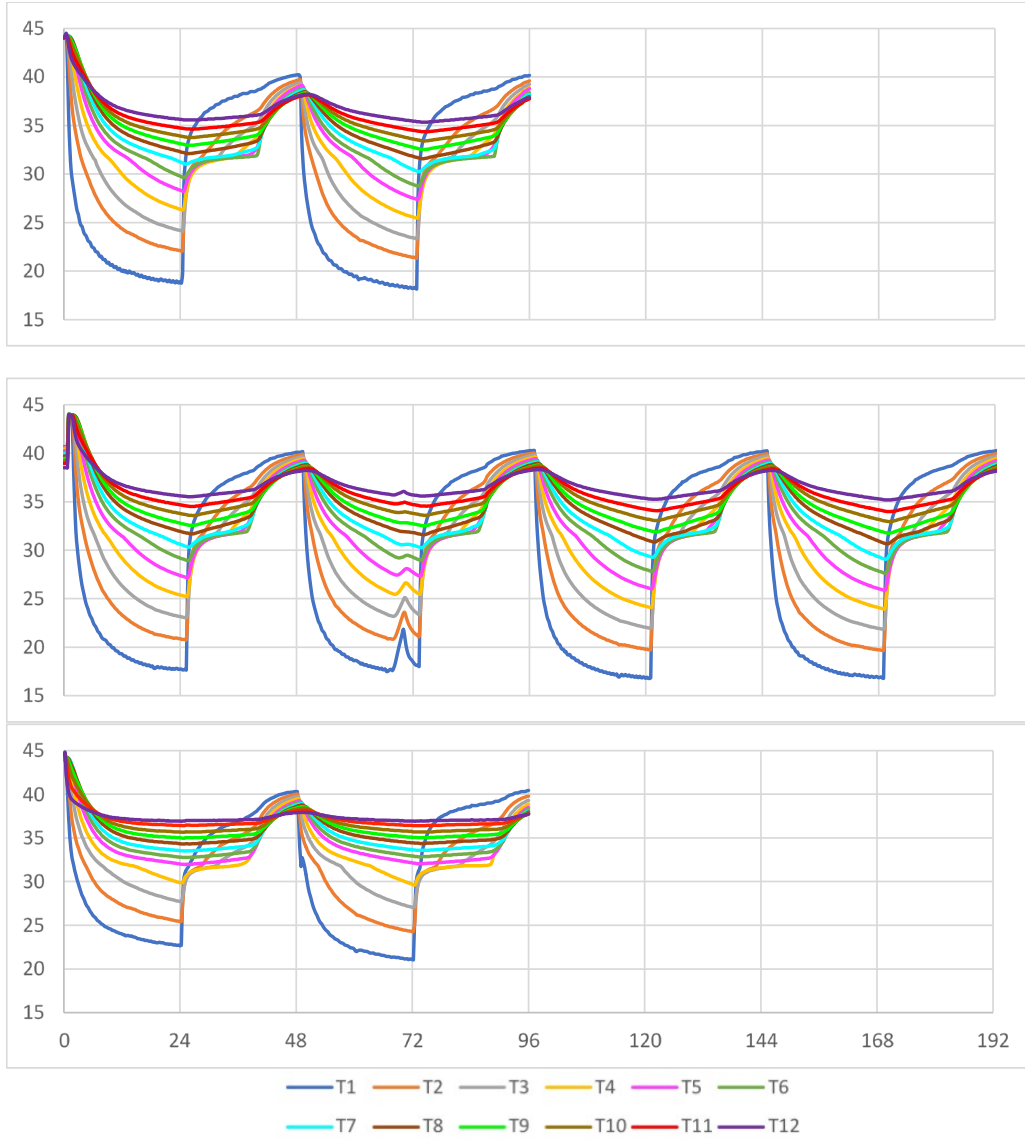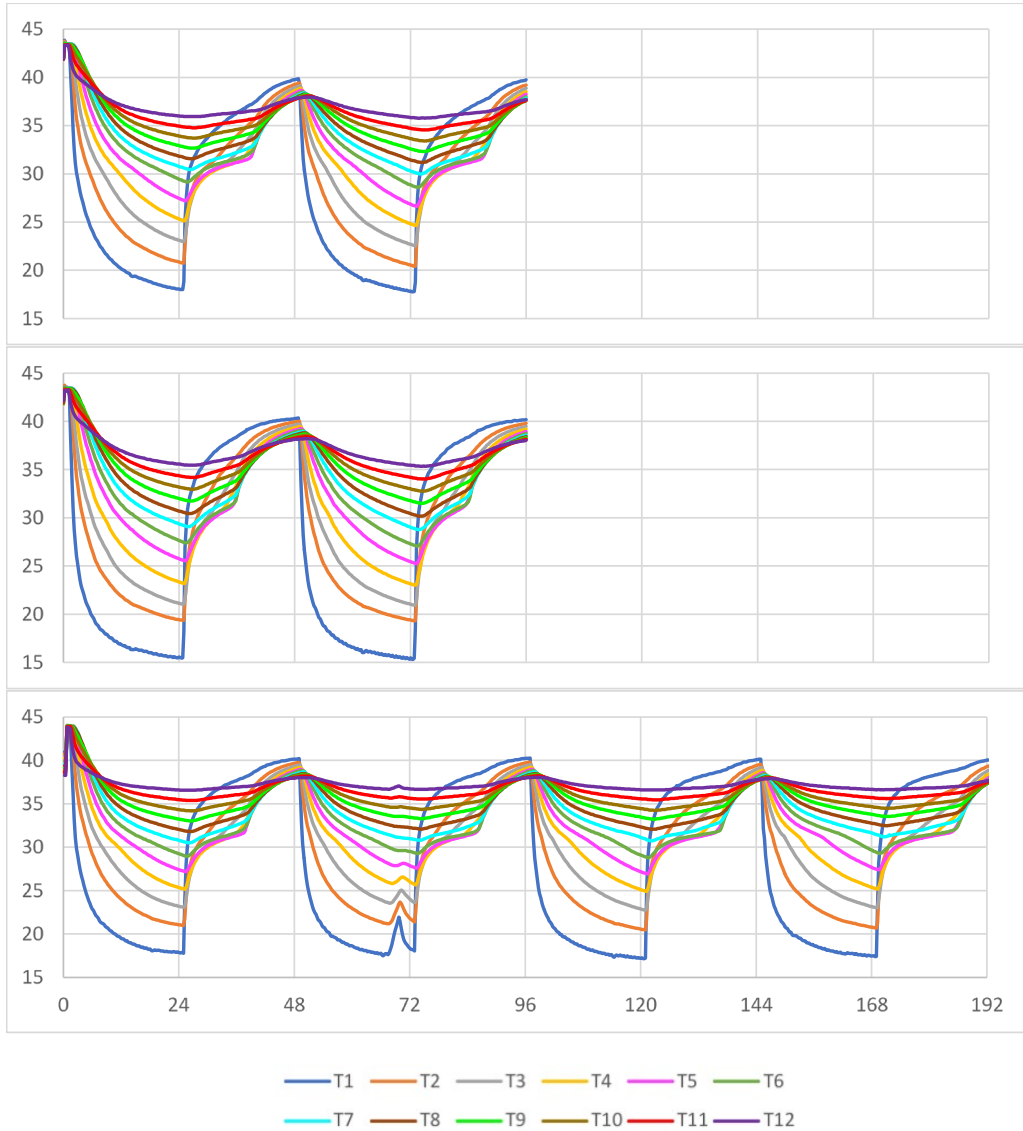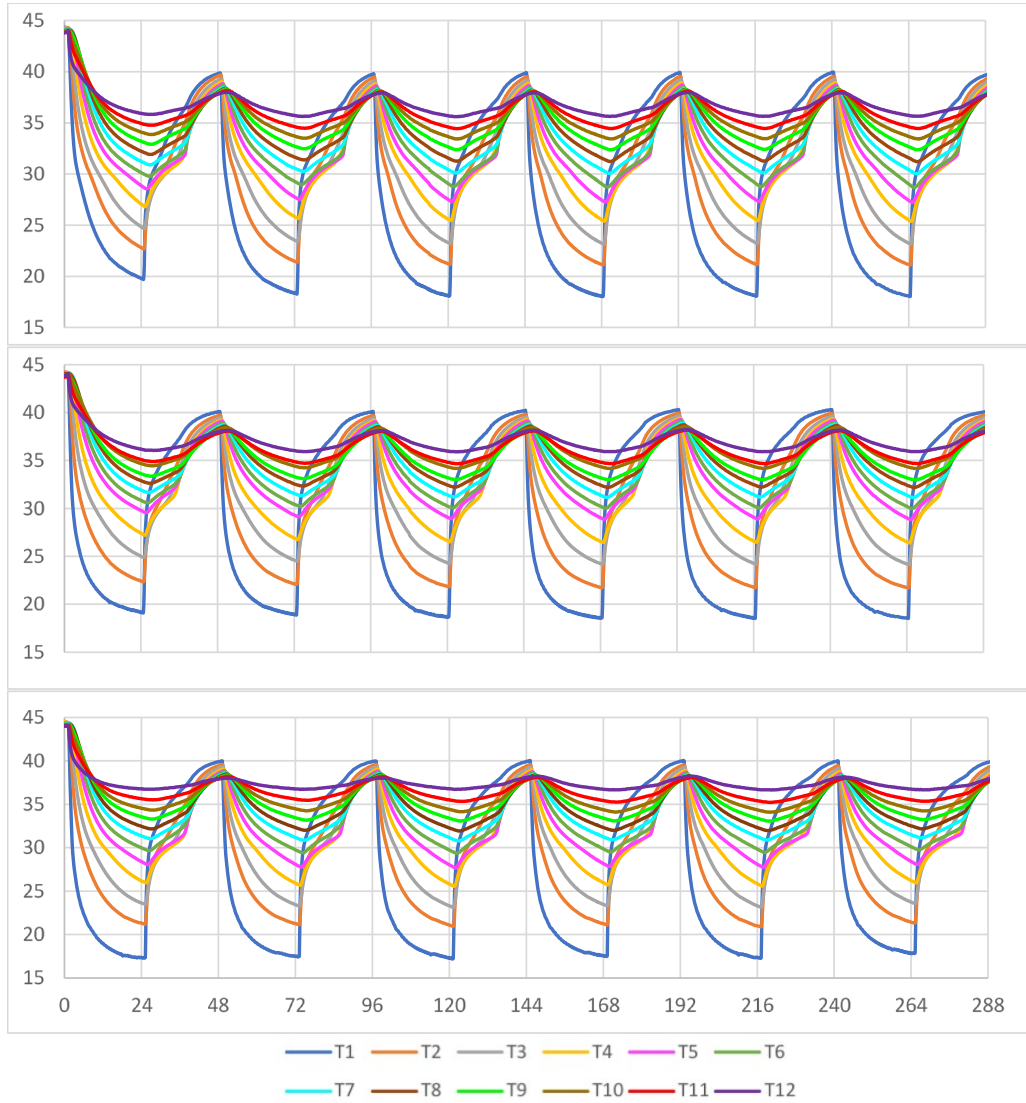
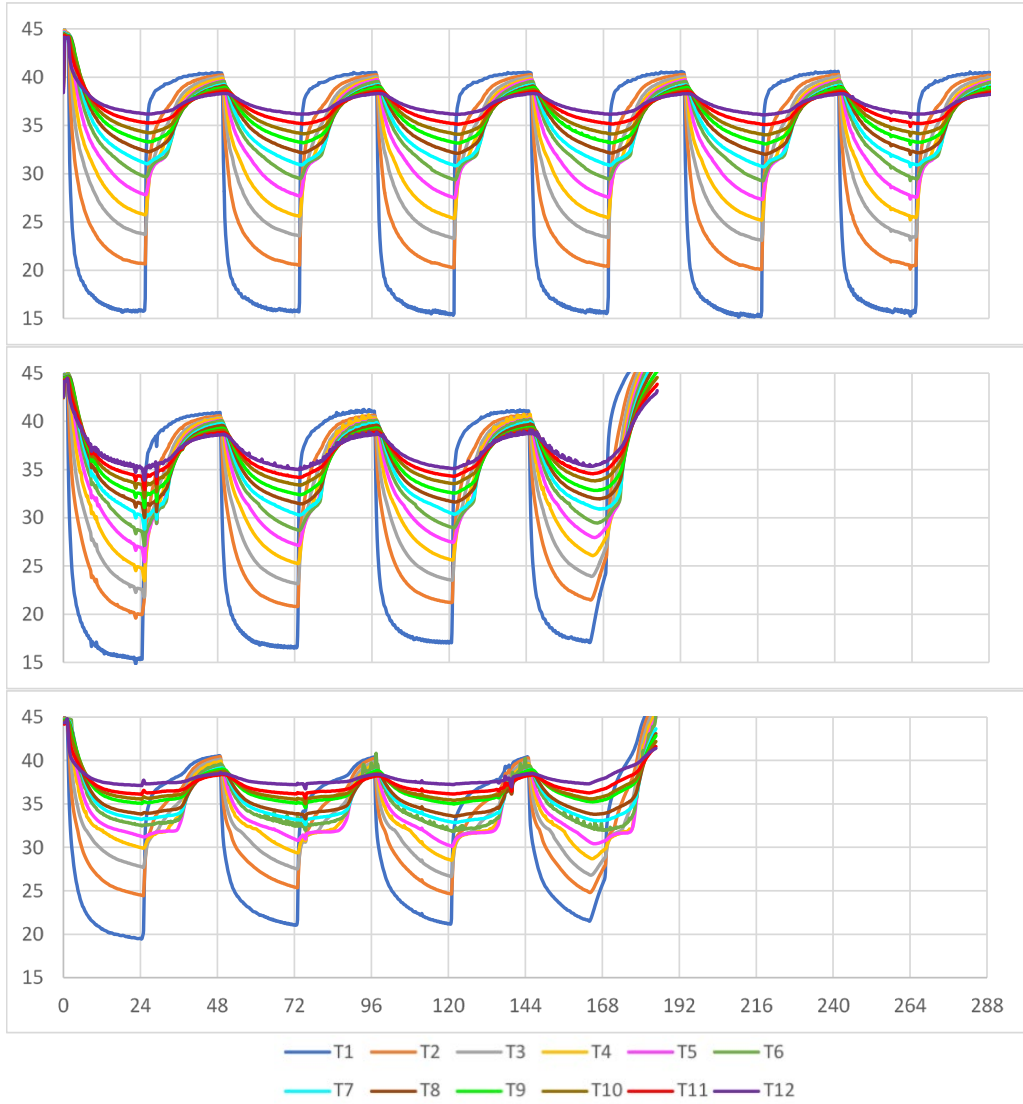Figure A-6. Replicate frost-heave layer temperatures (T1 = top, T12 = bottom) for soil type CL. Top, optimum moisture content; middle, 10% lower than optimum moisture content; bottom, optimum moisture content with free water added. The horizontal axis is time in hours. The vertical axis is layer temperature in degrees Fahrenheit. The anomaly in the bottom graph at approximately 72 hours was an unexpected power outage.
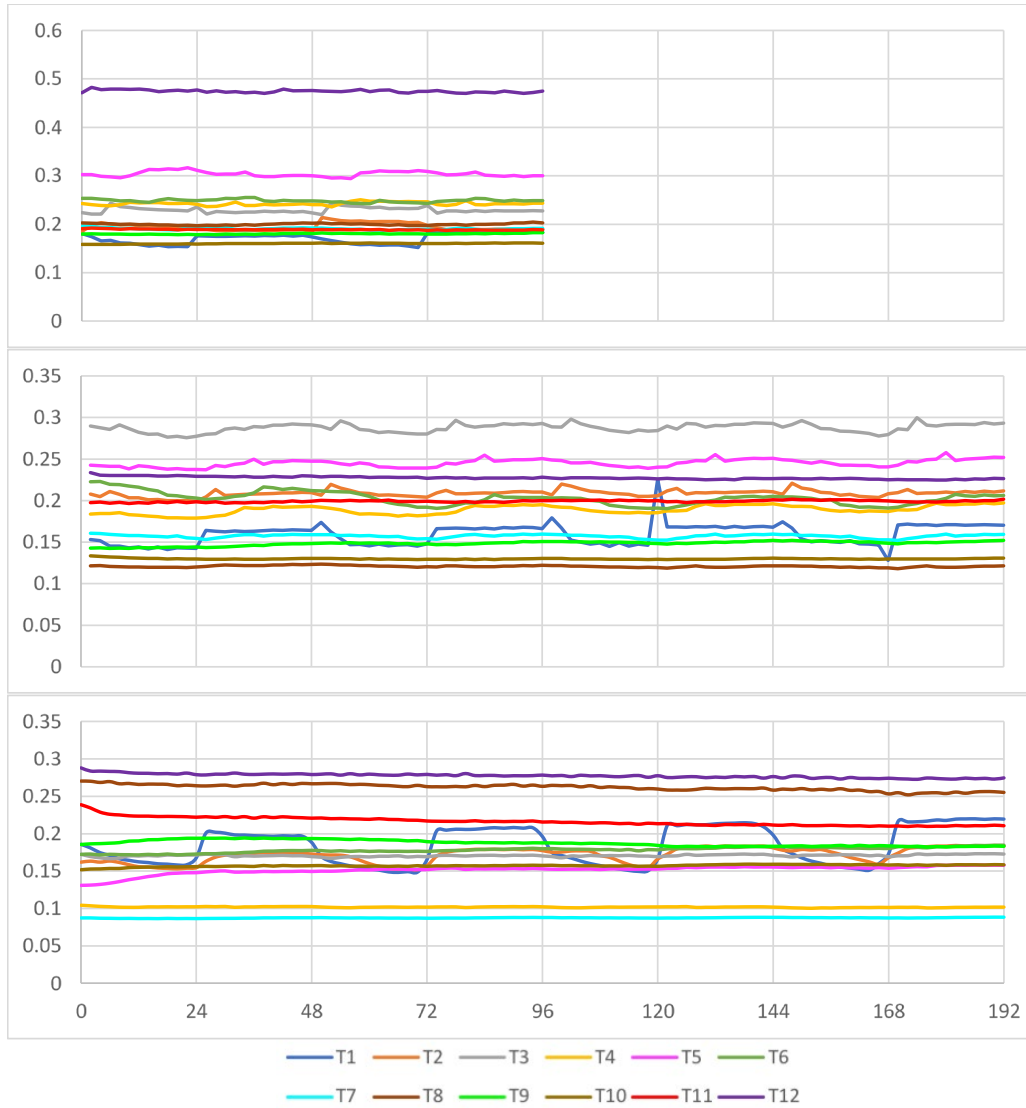
Figure A-7. Replicate frost-heave layer temperatures (T1 = top, T12 = bottom) for soil type CH. *Top*, optimum moisture content; *middle*, 10% lower than optimum moisture content; *bottom*, optimum moisture content with free water added. The horizontal axis is time in hours. The vertical axis is layer temperature in degrees Fahrenheit.

Figure A-8. Replicate frost-heave layer temperatures (T1 = top, T12 = bottom) for soil type SP. *Top*, optimum moisture content; *middle*, 10% lower than optimum moisture content; *bottom*, optimum moisture content with free water added. The horizontal axis is time in hours. The vertical axis is layer temperature in degrees Fahrenheit. The anomaly in the middle and bottom graphs at approximately 164 hours was an unexpected power outage.
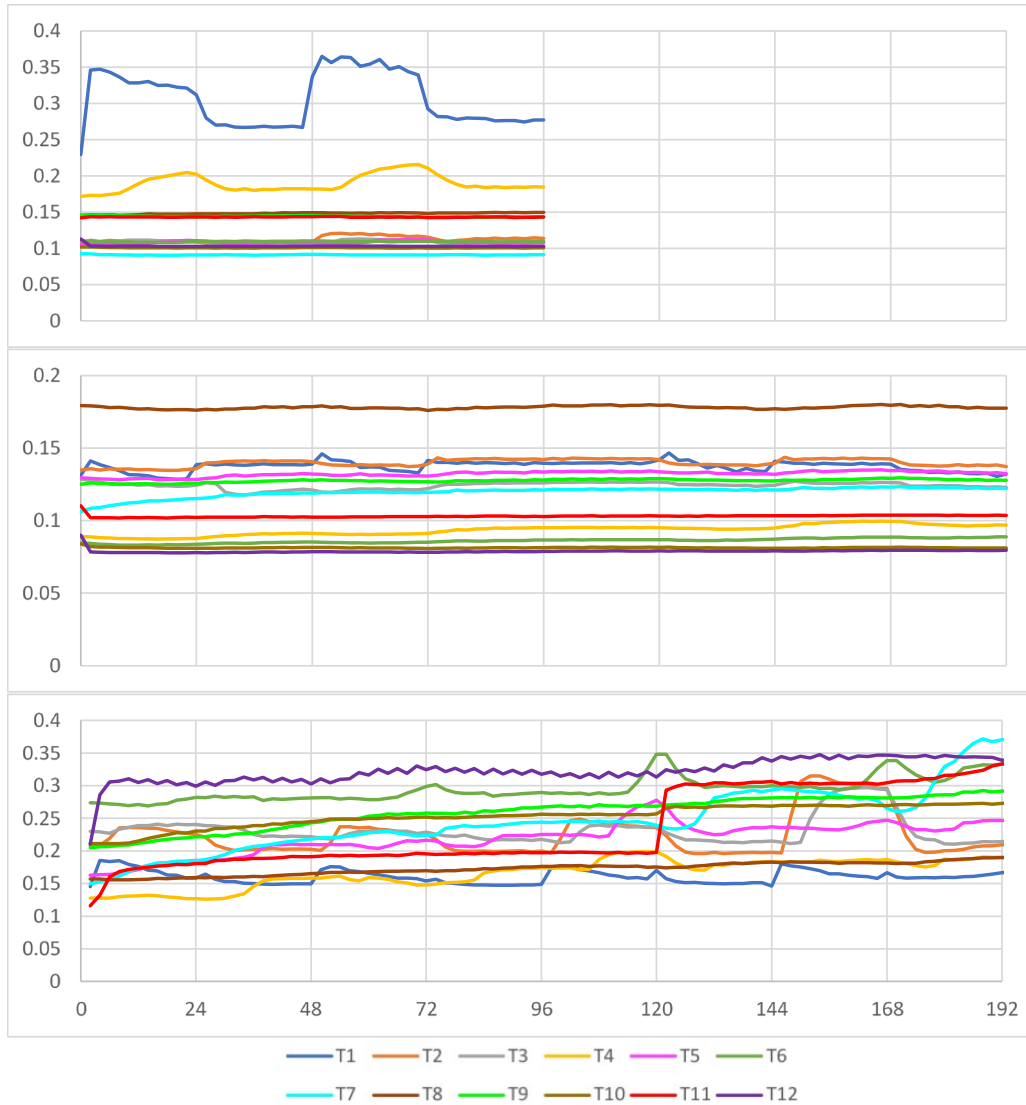
Figure A-9. Replicate frost-heave layer conductivities (T1 = top, T12 = bottom) for soil type ML. *Top*, optimum moisture content; *middle*, 10% lower than optimum moisture content; *bottom*, optimum moisture content with free water added. The horizontal axis is time in hours. The vertical axis is layer conductivity in Btu/(hr*ft*°F). The anomaly in the middle graph at approximately 72 hours was an unexpected power outage.

Figure A-10. Replicate frost-heave layer conductivities (T1 = top, T12 = bottom) for soil type CL. *Top*, optimum moisture content; *middle*, 10% lower than optimum moisture content; *bottom*, optimum moisture content with free water added. The horizontal axis is time in hours. The vertical axis is layer conductivity in degrees Fahrenheit. The anomaly in the bottom graph at approximately 72 hours was an unexpected power outage.

Figure A-11. Replicate frost-heave layer conductivities (T1 = top, T12 = bottom) for soil type CH. *Top*, optimum moisture content; *middle*, 10% lower than optimum moisture content; *bottom*, optimum moisture content with free water added. The horizontal axis is time in hours. The vertical axis is layer conductivity in Btu/(hr*ft*°F).
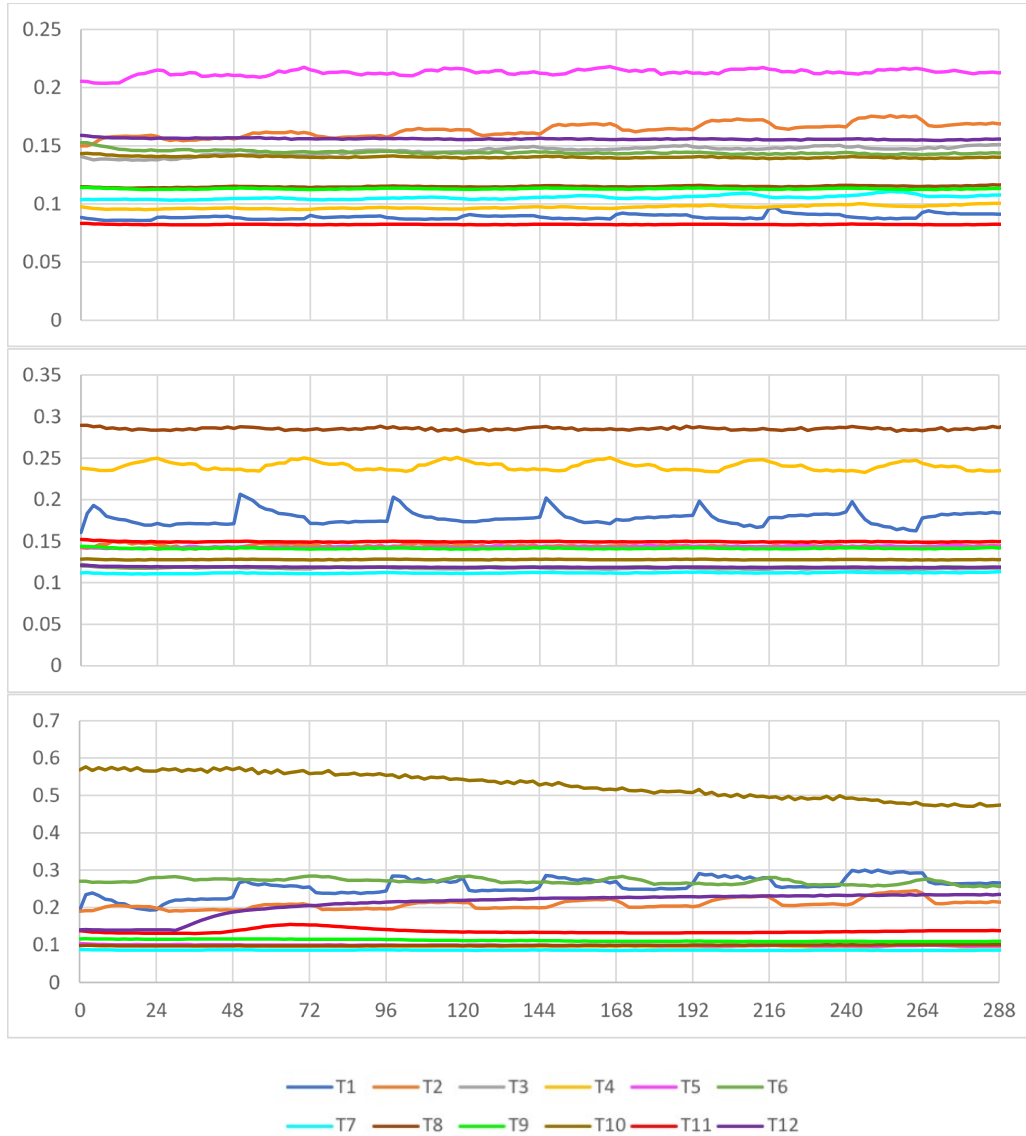
Figure A-12. Replicate frost-heave layer conductivities (T1 = top, T12 = bottom) for soil type SP. *Top*, optimum moisture content; *middle*, 10% lower than optimum moisture content; *bottom*, optimum moisture content with free water added. The horizontal axis is time in hours. The vertical axis is layer conductivity in in Btu/(hr*ft*°F).
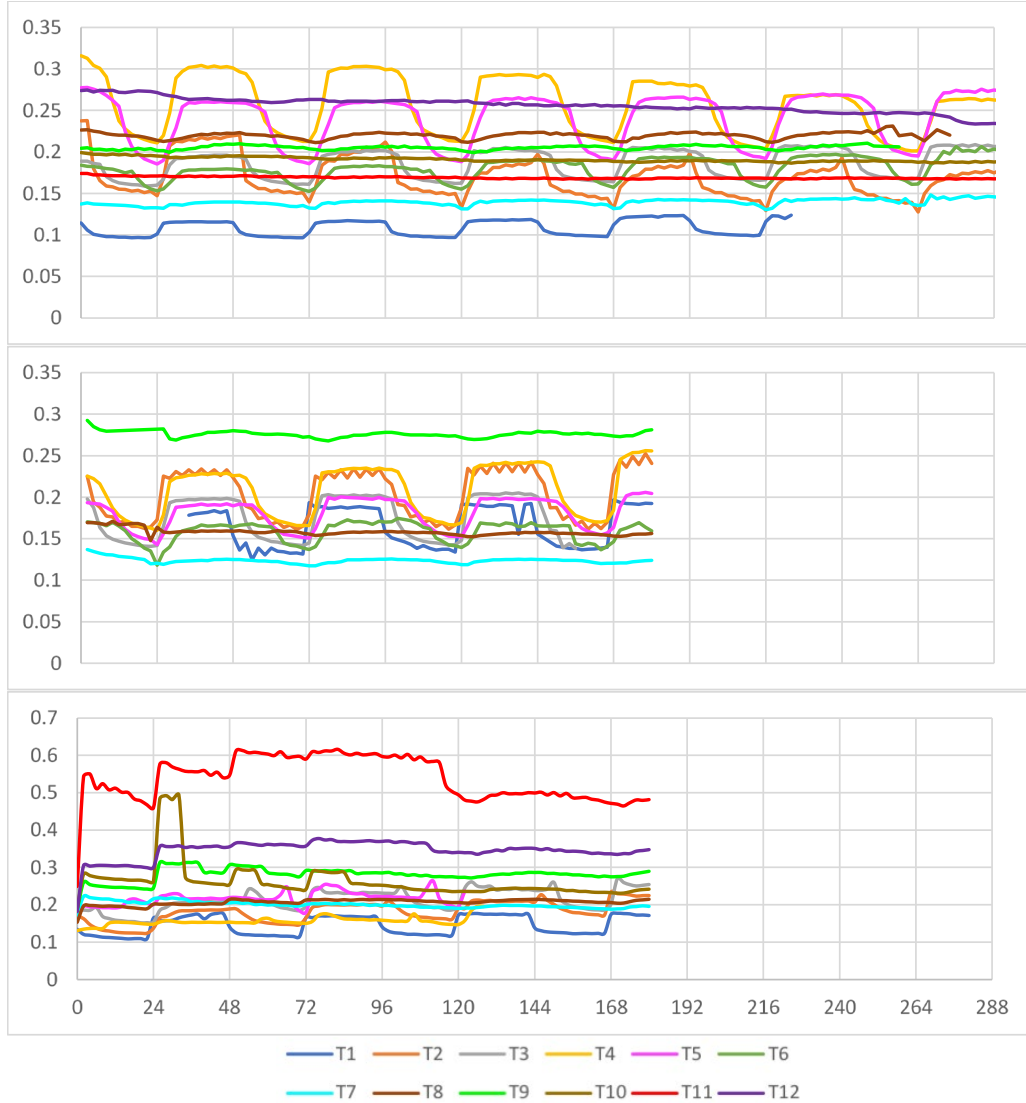
Figure A-13. Replicate frost depth and heave for soil type ML for all three moisture conditions.
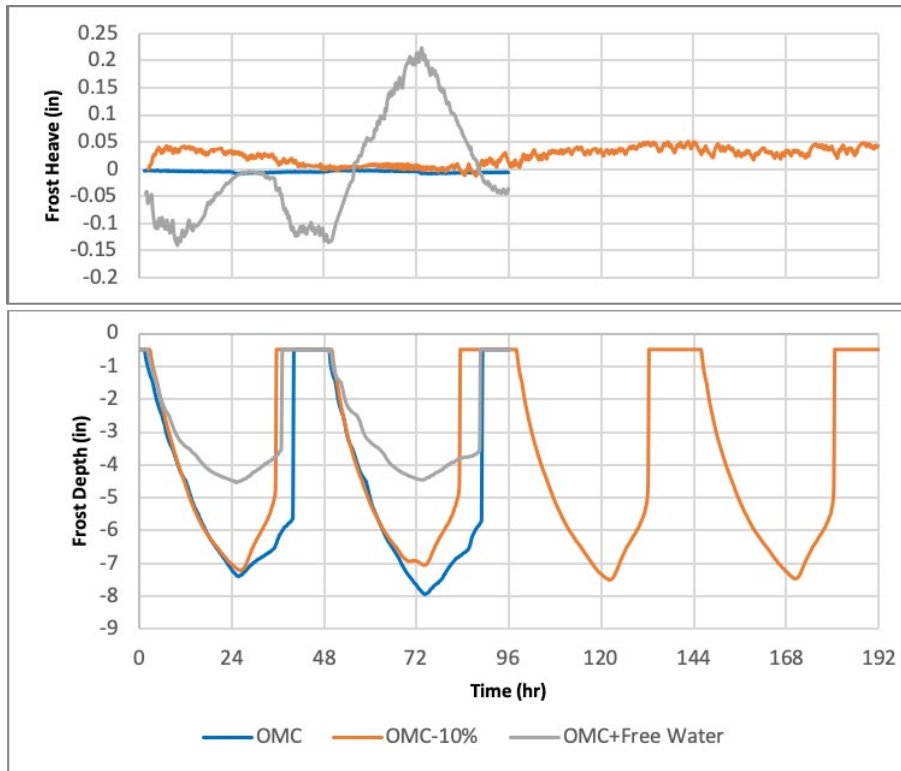
Figure A-14. Replicate frost depth and heave for soil type CL for all three moisture conditions.
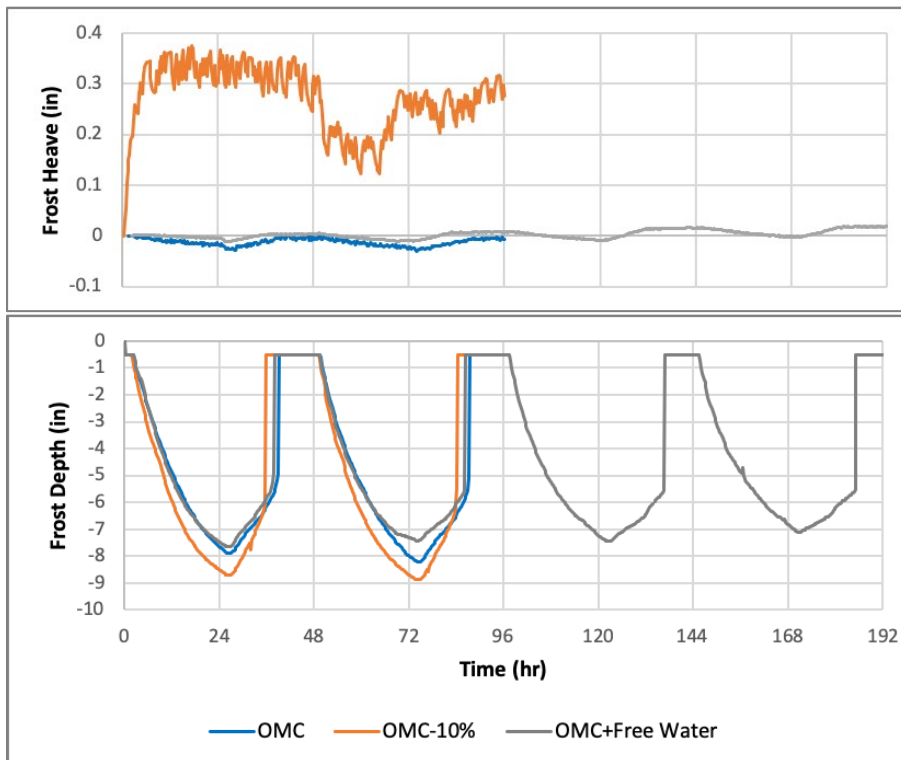
Figure A-15. Replicate frost depth and heave for soil type CH for all three moisture conditions.
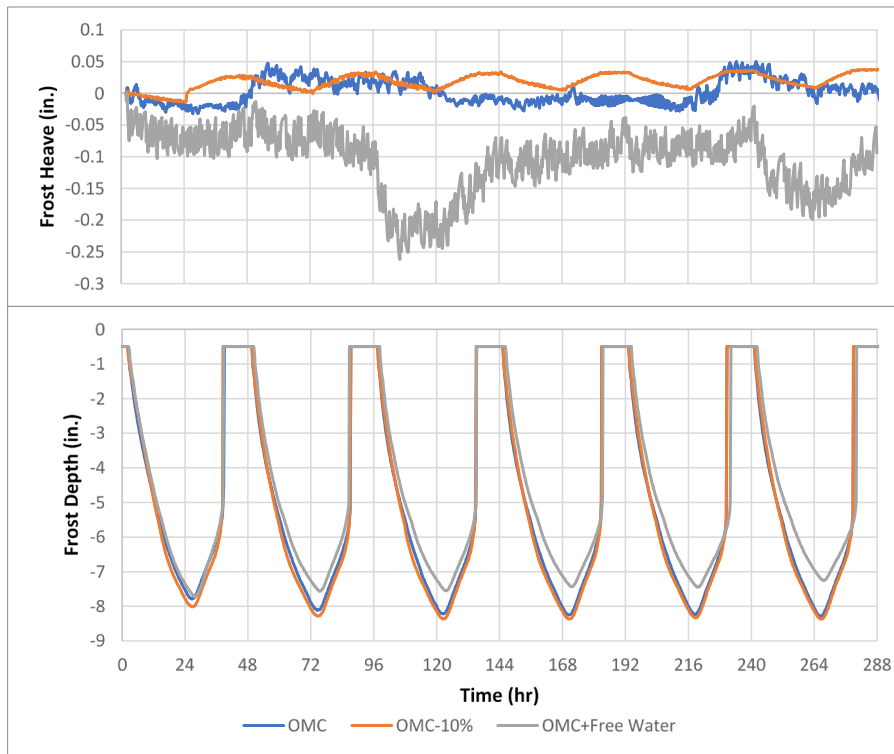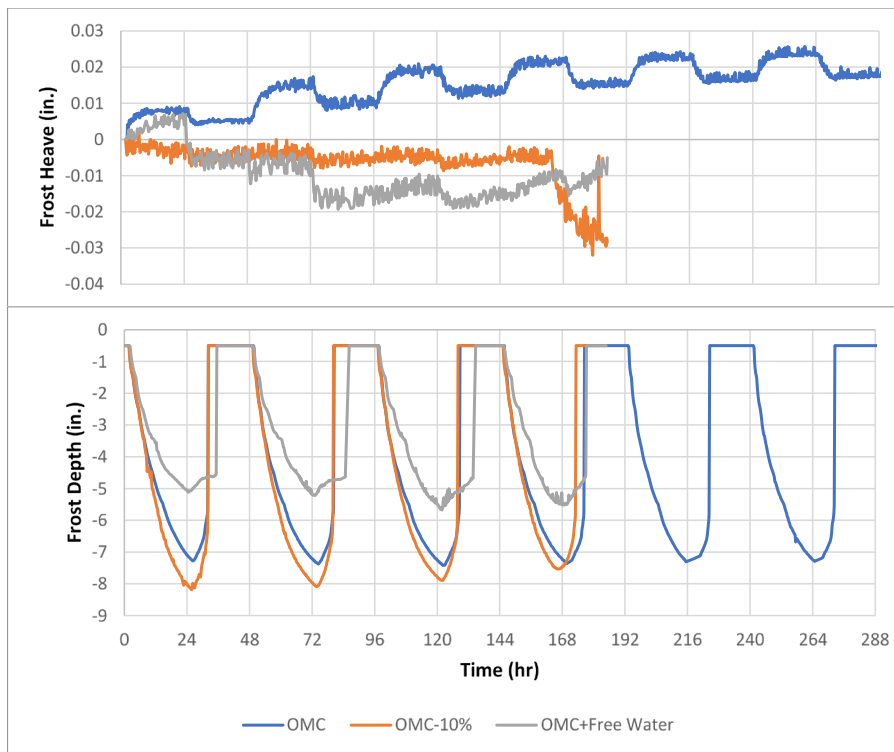

Figure A-16. Replicate frost depth and heave for soil type SP for all three moisture conditions.

REPORT DOCUMENTATION PAGE

1. REPORT DATE *(DD-MM-YYYY)*	2. REPORT TYPE	3. DATES COVERED *(From - To)*
November 2019	Technical Report/Final	

4. TITLE AND SUBTITLE

Frost-Depth Penetration and Frost Heave in Frost-Susceptible Soils

5a. CONTRACT NUMBER

5b. GRANT NUMBER

5c. PROGRAM ELEMENT NUMBER
62784

6. AUTHOR(S)

Wade A. Lein, Scott Michael L. Slone, Charles E. Smith Jr., Andrew P. Bernier, and Jared I. Oren

5d. PROJECT NUMBER
T53

5e. TASK NUMBER

5f. WORK UNIT NUMBER

7. PERFORMING ORGANIZATION NAME(S) AND ADDRESS(ES)

U.S. Army Engineer Research and Development Center (ERDC)
Cold Regions Research and Engineering Laboratory (CRREL)
72 Lyme Road
Hanover, NH 03755-1290

8. PERFORMING ORGANIZATION REPORT NUMBER

ERDC/CRREL TR-19-24

9. SPONSORING / MONITORING AGENCY NAME(S) AND ADDRESS(ES)

Headquarters, U.S. Army Corps of Engineers
Washington, DC 20314-1000

10. SPONSOR/MONITOR'S ACRONYM(S)

USACE

11. SPONSOR/MONITOR'S REPORT NUMBER(S)

12. DISTRIBUTION / AVAILABILITY STATEMENT
Approved for public release; distribution is unlimited.

13. SUPPLEMENTARY NOTES

14. ABSTRACT
The natural freezing and thawing of soils dramatically affects their thermal and mechanical properties. This can have destructive effects on structures built on those soils.

This study developed a thermodynamic finite element model using multiple frost-susceptible soil types. It measured thermal conductivity and temperature through several freeze–thaw cycles. We identified moisture migration as likely the most significant factor in frost heave and frost penetration. Additionally, the thermal conductivity increased near the freezing front across all samples. For example, the thermal conductivity for ML (low-plasticity silt) soils rose from 301 to 357 milliBtu/(hr*ft*°F), which appeared to correspond to where the moisture concentrated and ice formation was highest.

Our experimental results guided model development, where thermal parameters changed with respect to temperature, ice, and moisture during freeze–thaw cycles. Using dynamic thermal parameters improved frost-depth prediction compared to the standard Modified Berggren equation. For our tested conditions, the equation had an error of 2.2 in. for a frost depth of 8 in. while our model had an error of 1.4 in.

These developments are important to airfield runway and general pavements design and maintenance in frost-affected regions. The findings will allow more accurate predictions of frost depth and deflection.

15. SUBJECT TERMS
Finite element method, Frost depth, Frost heave, Frost heaving, Thermodynamics, Soils--Cold weather conditions, Soils--Effect of temperature on, Soil mechanics

16. SECURITY CLASSIFICATION OF:			17. LIMITATION OF ABSTRACT	18. NUMBER OF PAGES	19a. NAME OF RESPONSIBLE PERSON
a. REPORT	**b. ABSTRACT**	**c. THIS PAGE**	SAR	70	**19b. TELEPHONE NUMBER** *(include area code)*
Unclassified	Unclassified	Unclassified			